https://doi.org/10.5194/egusphere-2026-595
Preprint. Discussion started: 13 March 2026

Hyperlocal air quality monitoring and source apportionment of non-refractory $PM_{2.5}$ at three urban sites using stationary van-based measurements: A Lucknow case study

Davender Sethi[1], Akanksha Lakra[1], Ambasht Kumar[1], Shoubhik Chakraborty[1,3],Himadri Sekhar Bhowmik[1,4], Vaishali Jain[1,5], and Sachchida Nand Tripathi[1,2*].

[1]Department of Civil Engineering, Indian Institute of Technology Kanpur, Kanpur, 208016, India.
[2]Department of Sustainable Energy Engineering, Indian Institute of Technology Kanpur, Kanpur, 208016, India.
[3]Department of Computer Science and Engineering, Shiv Nadar University, Chennai, 603110, India.
[4] Institute of Climate and Energy Systems (ICE) - Troposphere (ICE - 3),Forschungszentrum Jülich GmbH,52428 Jülich, Germany.
[5]Atmospheric Chemistry, Max Planck Institute for Chemistry, Mainz, 55128, Germany.

Correspondence to: Sachchida Nand Tripathi(snt@iitk.ac.in)

Abstract. The present study addresses a key gap in characterizing hyperlocal air quality across three contrasting land-use settings during the peak pollution season in a central city in the Indo-Gangetic Plain (CIGP). We conducted ~744 hours of hyperlocal measurements in Lucknow city, spanning the post-monsoon to winter season over 31 days, using a Van-Based Stationary Ambient Air Quality Monitoring Platform (VSAAQMP). Measurements were conducted at three contrasting land-use settings—a background Site ("Site 1"), a traffic corridor ("Site 2"), and a major industrial cluster ("Site 3"). High-resolution time-of-flight aerosol mass spectrometer (HR-ToF-AMS) organic and inorganic mass spectra were subjected to Multilinear Engine-2, Positive Matrix Factorization (ME-2 PMF) source apportionment using a unified organic-inorganic aerosol (OA–IA) matrix. Across sites, NR-$PM_{2.5}$ was dominated by secondary organic aerosols (SOA), with biomass burning, traffic, and inorganic-associated organic factors (sulphate, nitrate-rich OA). Unlike Sites 1–2 (sulphate/low-volatility oxygenated organic aerosol (OOA)-dominant), Site 3 showed heterogeneous OA from biomass burning, semi-volatile/nitrate OOA, solid fuel, and traffic. Particle growth events (PGEs) were predominantly nocturnal, occurring under stable boundary-layer and inversion conditions. Site 3 exhibited ~5 times more nocturnal PGEs than the background, which was attributed to a higher condensation sink (CS). Stack vapors drive these PGEs (5–15 nm/h), enhancing the growth of oxidized biomass-burning organic aerosols (O-BBOA) and low-volatility OOA under inversions (r = 0.24). These results highlight the potential of near-source stationary van-based measurements for resolving hyperlocal aerosol growth processes and source influences.

https://doi.org/10.5194/egusphere-2026-595
Preprint. Discussion started: 13 March 2026

Keywords: Source Apportionment, Hyperlocal Monitoring, organic aerosols, Condensation sink, Particle growth events.

1. Introduction

Air pollution has emerged as a critical public health crisis in South Asia, contributing to millions of premature deaths each year. India bears one of the region's heaviest burdens, with approximately 1.67 million annual deaths linked to air pollution (Jaganathan et al., 2024). Persistent exposure to fine particulate matter—$PM_{2.5}$, defined as particles smaller than 2.5 μm—remains widespread, as India ranks among the highest globally in population-weighted $PM_{2.5}$ concentrations (Xu et al., 2025). These challenges are especially pronounced in the Indo-Gangetic Plain (IGP), including the understudied Central IGP, home to some of the world's most polluted cities (Hao et al., 2025; IQAir, 2023; Lakra et al., 2024) .

Organic aerosols represent a substantial fraction of $PM_{2.5}$ across South Asia, as consistently demonstrated in recent observational studies (Hao et al., 2025; Lakra et al., 2024; Shukla et al., 2025). Globally, OA typically represents 20–60% of fine aerosol mass and can exceed 90% in biogenically dominated environments such as tropical forests (Aktypis et al., 2024). This widespread presence reflects not only their atmospheric abundance but also their active role in shaping aerosol behavior. Organic aerosols participate in processes such as new particle formation and subsequent growth (Kerminen et al., 2018), undergo complex aging, and influence atmospheric radiation and climate (Seinfeld and Pandis, 2006). Understanding where these aerosols come from, how they transform, and how they vary over time is therefore essential for interpreting $PM_{2.5}$ levels and assessing their broader environmental and health implications (Liu et al., 2024a). These processes are governed by contributions from both primary and secondary organic aerosol components. Primary organic aerosols (POA) are directly emitted into the atmosphere from sources like vehicular exhaust, biomass burning, and fuel combustion (Du et al., 2018). In contrast, secondary organic aerosols (SOA) form in the atmosphere when precursor gases such as sulfur dioxide (SO_2), nitrogen oxides (NO_x), and ammonia (NH_3), and volatile organic compounds (VOCs)—undergo oxidation and produce low-volatility compounds, which then condense onto existing particles or nucleate to create new ones (Gu et al., 2023; Zhao et al., 2019). The types and amounts of emissions created can vary with ambient conditions. When VOCs undergo atmospheric oxidation, this process is closely linked to increases in particle diameter over time (Bhowmik et al., 2022; Jain et al., 2023). The resulting chemical transformations significantly influence the size and mass of $PM_{2.5}$ particles (Lalchandani et al., 2021).

Analyzing $PM_{2.5}$ composition reveals which species, such as sulfates, nitrates, ammonium, and organic compounds, contribute to hygroscopic and chemical growth(Kumar Kompalli et al., 2014). Variations in growth rates reflect the dynamic atmospheric processes that influence particle size distribution, toxicity, and health impacts (Schneider et al., 2015; Yue et al., 2009). Quantitative estimates of growth rates link chemical transformations with physical particle

https://doi.org/10.5194/egusphere-2026-595
Preprint. Discussion started: 13 March 2026

evolution, aiding source identification, exposure assessment, and air quality management (Kompalli et al., 2020; Kumar Kompalli et al., 2014; Mishra et al., 2023).

Previous research has noted that air quality is a problem at different length scales (Roychowdhury et al., 2023). The conventional method of monitoring and managing air quality worldwide, including in India, relies on satellite observations and fixed-site Continuous Ambient Air Quality Monitoring Stations (CAAQMS)(Sathe et al., 2020). However, the approach falls short in capturing the disproportionate exposure caused by intense emissions near their sources, which occur on the neighborhood scale (Barmpounakis et al., 2020). Consequently, it limits our understanding of intra-urban variability, fine spatial resolution, and hyperlocal gradients of various criteria pollutants, thereby hindering accurate health risk assessments within a region (Frederickson et al., 2023). There is a pressing need to conduct measurements at the hyperlocal level, characterizing particulate matter (PM) not only by mass concentration but also by its chemical composition, which critically influences its toxicity. Studies related to probing pathways of SOA formation and SOA were conducted earlier at Northern and CIGP Sites, primarily in Delhi (Bhattu et al., 2024; Bhowmik et al., 2022; Lalchandani et al., 2021, 2022; Shukla et al., 2021; Tobler et al., 2020). Furthermore, none of these studies used stationary van-based measurements to investigate hyperlocal air quality patterns across the city; only a few specifically analyzed intra-urban variabilities in NR-$PM_{2.5}$ composition. The stationary van-based measurements directly reflect air quality conditions along and near the roadways it surveys, providing localized, spatially resolved pollution data at the hyperlocal scale (Dhandapani et al., 2024; Lakra et al., 2025). The van used in the present study is equipped with highly sophisticated instruments, including an HR-TOF-AMS, an X-ray fluorescence-based metal monitor (Xact-625i), a Micro-Aethalometer, a scanning mobility particle sizer (SMPS), an optical particle sizer (OPS), and supporting instruments, such as pollutant gas analyzers and a Vaisala. Additionally, all measurements are stationary laboratory measurements with maximum characteristics at only four Sites in the CIGP, specifically in the city (Lakra et al., 2025). This study is the first of its kind in the CIGP, presenting source apportionment of NR-$PM_{2.5}$ at a hyperlocal scale across three Sites in Lucknow, India, from post-monsoon to winter using VSAAQMP. Additionally, stationary van-based monitoring efforts remain limited nationwide (DeWitt et al., 2015; Kerckhoffs et al., 2025; Maslouski et al., 2023). The motivation for conducting this research over Lucknow from the fact that, as one of India's fastest-growing economies and its most populous state, Uttar Pradesh's rapid development makes it essential to gain insights into its air quality (PRS Legislative Research, 2025). This study aims to (1) characterize the chemical composition of NR-$PM_{2.5}$ aerosols at the hyperlocal scale. (2) identify and quantify source contributions using a bilinear model, (3) analyze the diurnal and temporal variability of sources, and (4) investigate the association between particle growth events and aerosol composition dynamics in a polluted urban environment. The novelty of the present work lies in its hyperlocal characterization of urban aerosol populations within the city scale, demonstrating that particle number and mass are dominated by traffic-related and secondary sources, and that subsequent particle growth is strongly driven by the interplay of organic and inorganic vapors. This type of hyperlocal measurement helps strategically target air pollution sources rather than implementing bulk measures. Additionally, more coordinated and systematic actions are essential to address air pollution in highly impacted areas. The research integrates source apportionment, elemental ratios, and long-range transport assessments

https://doi.org/10.5194/egusphere-2026-595
Preprint. Discussion started: 13 March 2026

to understand pollution dynamics and spatial variability, providing insights essential for targeted mitigation and exposure reduction strategies in complex urban environments.

2. Study Site, Instrumentation, and Methodology:

2.1 Monitoring Sites for hyperlocal measurements.

Hyperlocal air quality monitoring using the VSAAQMP was conducted at three distinct locations in Lucknow: the Council of Scientific and Industrial Research–Central Institute of Medicinal and Aromatic Plants (CSIR-CIMAP) (26.89°N, 80.98°E), designated as the background Site(Lakra et al., 2025); Babasaheb Bhimrao Ambedkar University (BBAU) (26.77°N, 80.92°E), a traffic-influenced Site due to proximity to Shaheed Path; and Talkatora (26.83°N, 80.88°E), classified as the industrial Site due to its proximity to the industrial area of Lucknow (Jain et al., 2024; Lakra et al., 2025). These designations were based on each Site's proximity to different pollution sources. The city experiences a continental climate, characterized by extremely hot summers with temperatures reaching up to 46 °C and cold winters with temperatures as low as 7 °C (IMD, 2012). According to recent projections, the population of Lucknow in 2025 is estimated to be around 4.13 million for the metropolitan area and about 4.12 million for the city itself (Jain et al., 2023; Lucknow, India Metro Area Population 1950-2025, 2025). Key pollutants, including particulate matter ($PM_{2.5}$ and PM_{10}), carbon monoxide (CO), nitrogen dioxide (NO_2), and sulfur dioxide (SO_2), frequently exceed national ambient air quality standards in Lucknow (Jain et al., 2023; Pal et al., 2023). The first measurement Site, CSIR-CIMAP Lucknow, is located near the Kukrail forest in the northeastern part of the city, surrounded by a blend of urban development and green spaces. The Kukrail forest serves as a vital "green lung" for the area, significantly enhancing the local environment by absorbing carbon dioxide and pollutants through its dense tree cover, thereby helping reduce the urban heat island effect and combating climate change. The second measurement Site was BBAU (26.77°N, 80.92°E) in Lucknow, near Shaheed Path, a major expressway that significantly impacts the local environment. While this proximity improves accessibility and urban connectivity, it also increases air pollution from traffic in the campus vicinity. The area around BBAU features expanding residential neighborhoods, which further contribute to the urban landscape and affect local microclimate conditions. The presence of the Shaheed Path increases vehicular emissions, potentially compromising air quality near the university, particularly during peak traffic periods. When combined with emissions from surrounding residential areas, this contributes to moderate air pollution in the area. The third monitoring Site is the city's Talkatora Industrial Area. The VSAAQMP system has been deployed at the receptor location, situated downwind of the Site (26.83°N, 80.88°E). The Talkatora area of Lucknow, characterized by a concentration of small- and medium-sized industries, faces significant environmental challenges stemming from industrial operations. Its surroundings feature a mix of industrial estates and residential neighborhoods, forming a complex urban-industrial environment. Industrial activities in Talkatora are a major source of air pollution, often resulting in "severe" pollution levels. Hereafter, throughout this manuscript, CIMAP (26.89°N, 80.98°E), BBAU (26.77°N, 80.92°E), and Talkatora (26.83°N, 80.88°E) are referred to as Site 1, Site 2, and Site 3, respectively.

https://doi.org/10.5194/egusphere-2026-595
Preprint. Discussion started: 13 March 2026

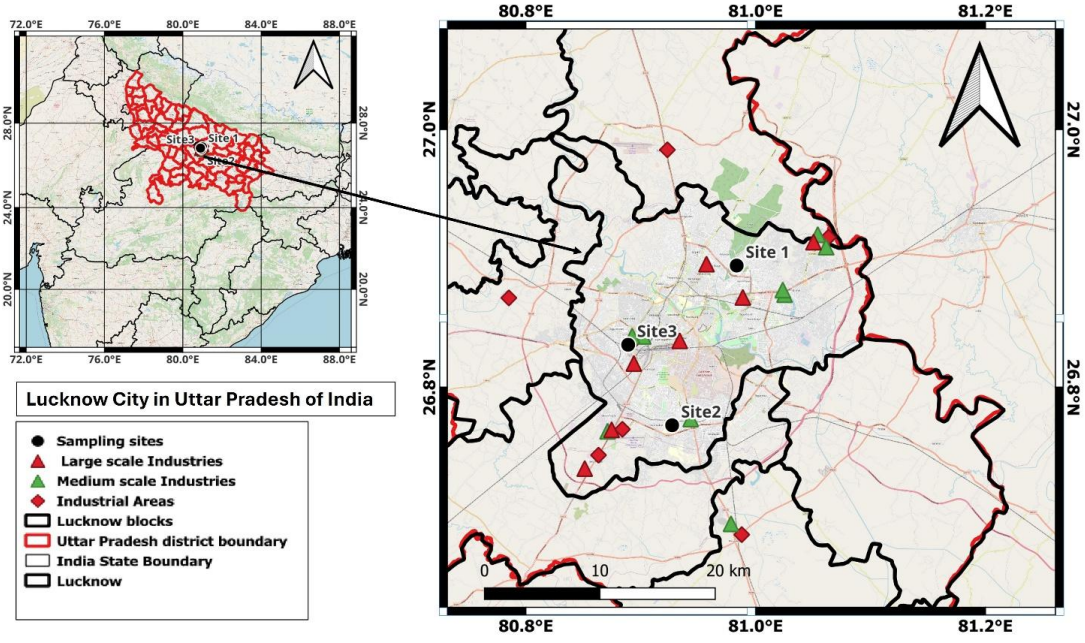

Figure 1. Showing the locations of the hyperlocal monitoring Sites in the city of Lucknow, Uttar Pradesh, India.

2.2 Sampling Period and Instrument Duration

The measurement was carried out from October to November 2023, during the post-monsoon season, across Lucknow, a major urban center in the CIGP. The measurement was carried out by deploying the VSAAQMP at a specific location for approximately 12-14 days, including 2-3 days for instrument calibration. However, the sampling duration has been extended in case of monitoring challenges, such as hardware failure, radio frequency interference to the AMS spectra, and van alignment with the road (Mushasha et al., 2024). Therefore, considering the above-mentioned challenges during the sampling period and filtering the noise from the measurement data, we have considered the measurement data for the CSIR-CIMAP for 6 days, i.e., from the 2nd of October 2023 to 7th October 2023, 11 days for 13th October 2023 to 23rd October 2023, and 14 days for 6th November 2023 to 19th November 2023, respectively. All instruments were well installed, rack-mounted, stable, and positioned on a stand with an AMS over a three-degree-of-freedom spring stand system. For more details on the VSAAQMP, the reader can refer to our study on the source apportionment of elements across Lucknow city, using the VSAAQMP (Lakra et al., 2025). The van was equipped with an air conditioning system to maintain an optimal temperature, with thermally insulated walls to ensure proper functioning of all instruments. The subsequent section describes the specifications and working principles of each instrument utilized in the study.

2.2.1 HR-ToF-AMS

https://doi.org/10.5194/egusphere-2026-595
Preprint. Discussion started: 13 March 2026

The Aerodyne Research Inc. HR-ToF-AMS was installed in a van to examine the chemical composition and size-resolved mass concentrations of NR-$PM_{2.5}$ particles at a 2-minute temporal resolution. The operational mechanisms of the HR-ToF-AMS are detailed in a research article (DeCarlo et al., 2006), and a brief overview is provided below. The inlet uses stainless-steel tubing (outer diameter ~8mm and inner diameter ~6 mm) to maintain a flow rate of 0.08 L/min. It is connected to a silica gel diffusion dryer, which reduces moisture by 20% before the air enters the instrument's main sampling inlet (Bhattu et al., 2024; Chakraborty et al., 2016; Tobler et al., 2020). The silica gel beads are recharged every 5-6 days after each Ion Efficiency (IE) calibration at the start of sampling at each Site, to prevent humidity from impacting particle collection efficiency. After that, the ambient aerosols were passed through the critical orifice of ~100µm and entered the sizing chamber by an aerosol dynamic lens. In this chamber, a high-vacuum environment was maintained, and the particle size was determined by measuring the time it took for particles to travel a fixed distance. They were vaporized into a gaseous state. The resulting gas molecules are then ionized with an electron ionizer at 70 eV, and the ions are subsequently detected by a multi-channel plate (MCP) detector. Through the sampling period, the instrument is operated in the V-mode at all three Sites, characterized by the low resolving power($m/\Delta m$ =~2500 for m/z 10-200,Δm is the full width half maximum, and m being the nominal m/z (DeCarlo et al., 2006) and high sensitivity (1-min detection limit of ~ 0.04 μgm^{-3}). The instrument performed two cycles during the 2-minute sampling interval, each lasting 30 seconds. These cycles alternated between mass spectrum (MS) mode, which involved 15 seconds blocked and 15 seconds open, and particle time-of-flight (PToF) mode, which ran for 30 seconds. Although we used MS data for our current analysis, we collected data in both MS and PToF modes to support potential future studies. The datasets obtained from the instrument from all three Sites were analyzed using SQUIRREL (SeQUential Igor data RetRiEvaL, version 1.66B) for Unit Mass Resolution (UMR) data and PIKA (Peak Integration by Key Analysis, version 1.26B) for high-resolution (HR) data. Both tools were implemented using IGOR Pro 9.0.5.4 (Wavemetrics, Inc., Portland, OR, USA), with a peak-fitting algorithm (DeCarlo et al., 2006) applied over m/z ratios from 12 to 120. Air interference correction was performed by adjusting the fragmentation table at specific mass-to-charge ratios (m/z) of 44,34, 33, 32, 18, 16, and 12. This process utilized data from high-efficiency particulate air (HEPA) filters, which were frequently collected during the sampling period (Aiken et al., 2008; Allan et al., 2004). A collection efficiency (CE) value of 1 was used for the capture vaporizer, as recommended by Hu et al. (2017). Calibrations, including ionization efficiency (IE), were conducted at the beginning of each sampling Site. These calibrations followed the mass-based method using a condensation particle counter (CPC) and a scanning mobility particle analyzer (SMPS), as described by Jayne et al. (2000). The calibrations used 300 nm monodisperse particles of ammonium nitrate (NH_4NO_3) for IE calibration and ammonium sulfate ($NH_4(SO_4)_2$) for RIE calibration with details provided in Table TS2 (a and b) of the supplementary information. Experimentally determined average relative ionization efficiencies (RIEs) for NH_4 and SO_4 at three Sites were 4.48 and 1.47, respectively. For chloride and organics, default RIE values of 1.3 and 1.4 were used in the present work. These defaults, established through laboratory calibrations with standards such as NH_4Cl and organic compounds (e.g., levoglucosan), are widely used when Site-specific calibration is unavailable due to their robustness across ambient conditions and consistency with inter-instrument comparisons (Khare et al., 2025; Watson et al., 2020). They ensure the reliable quantification of non-

https://doi.org/10.5194/egusphere-2026-595
Preprint. Discussion started: 13 March 2026

refractory species without overcomplicating the analysis, especially for low-concentration chlorides (often NH_4Cl), where custom RIE determination may lack sufficient signal-to-noise (Nuaaman et al., 2015).

2.2.2 Micro-Aethalometer:

The real-time BC mass concentrations were measured using a laboratory-calibrated Micro-Aethalometer (AethLabs, model AE51), a self-contained device equipped with built-in pumps, a battery, an internal memory card for data storage, and flow control (AethLabs, 2016). This device is tailored for exposure monitoring and quantifies the rate of change in light absorption due to the continuous buildup of aerosols on a T60 Teflon-coated glass fiber filter. Measurements at 880nm are used as an indicator of atmospheric BC concentrations. The instrument was regularly monitored to ensure data accuracy. The maintenance routine included checking the flow rate, monitoring screen warnings, and replacing the AE51 filter every 4-5 hours to prevent aerosol overloading (ATN≤100). This is important because high filter loading can cause BC levels to be underestimated (Weingartner et al., 2003). The instrument provides minute-by-minute high-resolution data, but we averaged over 30 minutes for analysis to reduce real-time data variability(Cheng and Lin, 2013). The laboratory-calibrated Micro-Aethalometer (AethLabs AE51) measures real-time BC mass with ±20% accuracy, ±5-10% precision, and ~1 μgm^{-3} detection limit (1-min average)(Alas et al., 2020). Uncertainties arise from filter loading (up to 70% bias without correction) and RH/T effects; apply by research (Virkkula et al., 2012) loading corrections for ±10-15% Root mean square error (RMSE) (Good et al., 2018). Furthermore, the instrument was placed on a stable base to minimize vibrations, and sampling was conducted through a separate silicon tubing inlet, which was regularly cleaned with a foam spray to remove any blockages and maintain optimal sampling conditions. Moreover, previous studies have shown a robust correlation for both collocated measurements (Alas et al., 2019; Vernooij et al., 2022).

2.2.3 SMPS

The particle size distributions (12–672 nm) along with particle count were measured using a SMPS comprising a TSI model 3082 electrostatic classifier, a long Differential Mobility Analyzer (DMA), and a TSI model 3776 Condensation Particle Counter (CPC)(TSI Incorporated, 2006). More details can be found in the previous papers(Lakra et al., 2024; Mishra et al., 2023)

2.2.4 Auxiliary Instruments and Parameters

Data on external factors, including trace gases and meteorological parameters such as ambient temperature (AT) in °C, relative humidity (RH) in %, and wind speed (WS) in ms^{-1}, were measured using collocated operational instruments inside the van, including gas analyzers and Vaisala sensors. Measurements of trace gases, such as ozone (O_3), sulfur dioxide (SO_2), carbon monoxide (CO), and nitrogen dioxide (NO_2), were measured using Thermo Scientific gas analyzers (models 49i, 43i, 48i, and 42i, respectively). All gas monitors were calibrated at the start of the campaign at each Site using a dynamic gas calibrator (model 146i). To validate the NR-$PM_{2.5}$ measurement data from the reference-grade $PM_{2.5}$ monitor, Environment Beta Attenuation Monitor (E-BAM), manufactured by MetOne. The used monitor is USEPA-certified and uses the beta attenuation technique to measure $PM_{2.5}$ particles (U.S. Environmental Protection

https://doi.org/10.5194/egusphere-2026-595
Preprint. Discussion started: 13 March 2026

Agency, 2025). We have used the PM_{10} inlet in conjunction with the $PM_{2.5}$ cyclone to robustly measure the $PM_{2.5}$ mass concentration in μgm^{-3}. The monitor used is a USEPA-certified device that employs the beta attenuation technique to measure $PM_{2.5}$ mass concentration. The Planetary Boundary Layer Height (PBLH) data from MERRA-2, with a spatial resolution of approximately 0.5° × 0.625° on a latitude-longitude grid and hourly temporal averaging for the sampling period, have been extracted for the Sites of interest (Gelaro et al., 2017).

2.3 Source Apportionment Analysis (SAA)

2.3.1 SAA using PMF

Several receptor models are available for analyzing the characteristics of ambient aerosol measurements (Air Pollutant Receptor Modeling, 2025; Watson et al., 2002). PMF with ME-2 engine was applied to the combined organic and inorganic aerosol mass spectra obtained using a HR-ToF-AMS at all three Sites. The reason for using PMF coupled with ME-2 was selected because it (i) uses an error-weighted, mass-conserving framework that incorporates individual measurement uncertainties, (ii) enforces non-negativity on both source profiles and contributions, leading to physically realistic factors, and (iii) allows the inclusion of a priori constraints in ME-2 to stabilize solutions and separate closely collinear sources more robustly than traditional models such as chemical mass balance (CMB) or unconstrained factor analysis (Paatero, 1999). The receptor model combines unconstrained factor exploration with a priori profile constraints (α = 0.02–0.1), achieving >95% OA mass closure, 50-70% reduced rotational ambiguity, and <20% uncertainty for major factors like HOA/OOA across Sites (Drosatou et al., 2019). It employs a bilinear unmixing algorithm with non-negative constraints, utilizing distinctive factorization (Paatero and Tapper, 1994), which involves iterative reweighting of the data to yield unique solutions, as shown in equation (1).

$$x = \sum_{k=1}^{p} g_{ik} f_{kj} + e_{ij} \quad (1)$$

In this context, x_{ij} represents the concentration of the j^{th} species in the i^{th} sample. The source profile of the k^{th} source to the j^{th} species is denoted by $f_{kj,}$ while g_{kj} represents the time series of the j^{th} species in the k^{th} source. The residual matrix is represented by e_{ij}, and the number of factors is denoted by p. To solve equation 1, the minimization of the quantity Q (as defined in the equation) is performed. The measurement uncertainty determines this quantity Q (σ_{ij}) and the elements of the residual matrix (e_{ij}) defined in equation (2).

$$Q = \sum_{l=1}^{n} \sum_{j=1}^{m} \left(\frac{e_{ij}}{\sigma_{ij}}\right) \quad (2)$$

Due to the rotational ambiguity inherent in PMF, multiple rotated solutions of the matrices F and G with similar Q-values can emerge, potentially resulting in mixed-factor solutions. To address this, PMF (Paatero, 1999) was implemented using the Source Finder interface (SoFi version 9.5.4.6, Datalystica Ltd., Villager, Switzerland) for source apportionment analysis, as described in research articles (Canonaco et al., 2013; Crippa et al., 2014). Additionally, the a-value in ME-2 was constrained to 0.5 for Sites 1 and 2 for the HOA factor. In this context, the a-value controls the allowed deviation of the optimized factor profiles from the selected reference profiles of HOA

https://doi.org/10.5194/egusphere-2026-595
Preprint. Discussion started: 13 March 2026

(Mohr et al., 2012). The a-value of 0.5 permits ±50% relative variation around the anchor profile, providing flexibility to capture Site-specific variability while preventing unrealistic drift of the solution. The constraint was implemented by supplying the reference profiles to ME-2 and specifying values for the corresponding factors, following the standard constrained PMF implementation in the SoFi/ME-2 framework (Shukla et al., 2025).

2.3.2 SAA of Combined Organic and Inorganic Aerosols

Using half-hourly averaged HR-ToF-AMS data from all three Sites, the high-resolution ions (m/z 12–120) were combined with unit mass resolution ions (m/z 121–300) extracted from organic aerosol mass spectra, along with several major inorganic ions. The inorganic ions included SO (m/z 47.97), SO_2 (m/z 63.96), SO_3 (m/z 79.96), HSO_3 (m/z 80.96), H_2SO_4 (m/z 97.97), NH (m/z 15.01), NH_2 (m/z 16.02), NH_3 (m/z 17.03), Cl (m/z 35.98), HCl (m/z 34.97), NO (m/z 29.99), and NO_2 (m/z 45.99). These ions were integrated to form the PMF input matrix, which consisted of 64769 sample points and 513 variables for Site 1, 131060 sample points with 507 variables for Site 2, and 137,228 sample points and 513 variables for Site 3, following procedures outlined in research articles (Sun et al., 2014; Ulbrich et al., 2009). Variables with a signal-to-noise ratio below two were down-weighted by a factor of 2, and those below 0.2 by a factor of 10. CO_2-related variables were excluded from the PMF analysis to prevent over-weighting the CO_2^+ variable, as these are calculated as constant fractions of the CO_2^+ signal in AMS data analysis(Lalchandani et al., 2022). This approach enabled the resolution of organic-rich factors, such as solid fuel combustion and biomass burning with diverse mass spectral characteristics, as well as traffic-related factors and oxygenated organic aerosol (OOA) factors, alongside inorganic-rich factors, at all three Sites. The combined organic and inorganic PMF resulted in clearly identified factors following the necessary selection of the optimal PMF solution (Lakra et al., 2024). The selection of factors was conducted according to the standard procedure followed in earlier studies (Akanksha et al., 2025; Bhowmik et al., 2022). For Site 1, PMF was explored for various factors, and a 7-factor solution was selected. For this configuration, repeated runs with different seeds and rotations yielded stable Q/Q_{exp} values of approximately 6–7, indicating a robust fit with minimal sensitivity to initialization. All seven factors (HOA, two BBOA factors, SV-OOA, LV-OOA, SO_4-OA, and NO_3-OA) showed physically interpretable profiles and time series, so this solution was adopted for further analysis. Similarly, the other factors are selected in a similar manner for other Sites.

2.3.3 Uncertainty Evaluation in PMF Solutions via Bootstrapping Analysis

To evaluate the uncertainty of the factor derived from the PMF model, a bootstrap resampling analysis (Paatero et al., 2014) was conducted in SoFi for each Site, with n = 1000 iterations, employing criteria-based selection (Brown et al., 2015). A balance between computational and statistical efficiency was achieved by using the initial 20 seed runs, which demonstrated good reproducibility of results across all three Sites (Brown et al., 2015; Cash et al., 2023; Srivastava et al., 2018; Vlachou et al., 2018). The base case for Site 1 was established from a bootstrapped time series of seven factors, including one constrained HOA factor and six unconstrained factors. For Site 2, the base case comprised six factors (one HOA-constrained and five unconstrained), while Site 3 used seven fully unconstrained

https://doi.org/10.5194/egusphere-2026-595
Preprint. Discussion started: 13 March 2026

factors. For each Site, Pearson's correlation coefficient (R) was calculated between the base-case factor time series and the randomly positioned bootstrap factors, and these R values were used to define the criteria scores. In SoFi, a criterion that is used to reposition and sort unconstrained factors is treated as an active criterion, whereas a passive criterion only reports the score for the current factor position and does not influence the sorting; this is typically applied to constrained factors, whose position is already known a priori, and for which criteria are used only for monitoring. Active or passive status is assigned by the user in the criteria panel, where selected (highlighted) criteria are active, and all others remain passive. In this study, correlation-based criteria were applied to unconstrained factors, and factors with active criterion R values greater than 0.8 and statistically non-significant differences from the base case (p-values above 0.05 from the t-test) were retained as the final robust factors for interpretation (Rai et al., 2020). Over 90% of the unmixed (unconstrained) factors achieved correlation scores greater than 0.8 at all three Sites, and solutions with 7, 6, and 7 factors were retained for Sites 1, 2, and 3, respectively. For Site 1, the constrained HOA factor also met the selection criterion, with approximately 50% of its bootstrap realizations exceeding the R > 0.8 threshold, consistent with its weaker, more mixed traffic signature at this background Site (Shukla et al., 2021).

2.4 Analysis of Back Trajectories and Concentrated Weighted Trajectories

Trajstat model v4.1 was used to conduct back trajectory analysis, tracing the origins and pathways of sources influencing NR-$PM_{2.5}$ species and combining inorganic and organic aerosols. It uses the Global Data Assimilation System (GDAS) weekly files, which provide data at 1-degree resolution in latitude and longitude. The backward trajectories were computed every 3 hours at 500 m above ground level, thereby incorporating the average Planetary Boundary Layer Height (PBLH). These trajectories were then weighted using time-series data that combined organic and inorganic factors. Since similar concentration patterns were observed at given attitudes, the 500m altitude was chosen to ensure that the backward trajectories remained within the mixing layer (Ghosh et al., 2015; Jain et al., 2023; Rai et al., 2020). Further, the Concentrated Weighted Trajectory (CWT) model was applied to each source factor using 3-hour averaged time-series data. This averaging ensured compatibility with the GDAS output interval required for CWT analysis, which was performed using Zefir, an Igor-based interface, to identify air parcels contributing to elevated concentrations at the sampling Site (Petit et al., 2017), using equation (3).

$$CWT_{ij} = \frac{1}{\tau_{ij}} \sum_{k=1}^{N} C_k \, \tau_{jk} \qquad (3)$$

In this context, j and i represent longitude and latitude, respectively. The average concentration of the weighted trajectory in the ij^{th} cell is denoted by CWT_{ij} (in $\mu g\ m^{-3}$). Here, k is the trajectory index, N is the total number of trajectories, τ_{ijk} is the residence time of trajectory k in the ij^{th} cell, and C_k (in $\mu g\ m^{-3}$) is the measured concentration of the factor associated with trajectory k.

2.5 Estimation of the particle growth rates and condensation sink

We estimated the particle growth rates for sizes ranging from 12 nm to 672 nm using SMPS data collected across the three Sites. The growth rate is calculated using equation (4) is provided below

https://doi.org/10.5194/egusphere-2026-595
Preprint. Discussion started: 13 March 2026

$$GR = \frac{\Delta d}{\Delta h} \quad (4)$$

Here, d represents the geometric mean diameter, and h denotes the measurement time in hours (Pushpawela et al., 2018). The particle growth rate is measured in nanometers per hour(nm/hr). The condensation sink (CS) was determined from the particle number size distribution using equation (5).

$$CS = 2\pi D \sum \beta_i N_i d_i \quad (5)$$

where D is the diffusion coefficient of the vapor, β_i is the Fuchs–Sutugin correction factor in cm^2s^{-1} d_i is the diameter of particles in the size bin i in nm, and N_i represents their number concentration(Tuovinen et al., 2020). The calculation assumes that vapor condensation onto aerosol particles can be approximated by condensation onto stationary particles. This assumption holds when particle sizes are significantly larger than those of vapor molecules, and their diffusion is correspondingly slower. Here we have considered the approximate value of 0.07 cm^2s^{-1} , and 1, for the D and β_i respectively (Wang et al., 2020).

3. Results and Discussion:

3.1 $PM_{2.5}$ Composition during campaign using MAQMS.

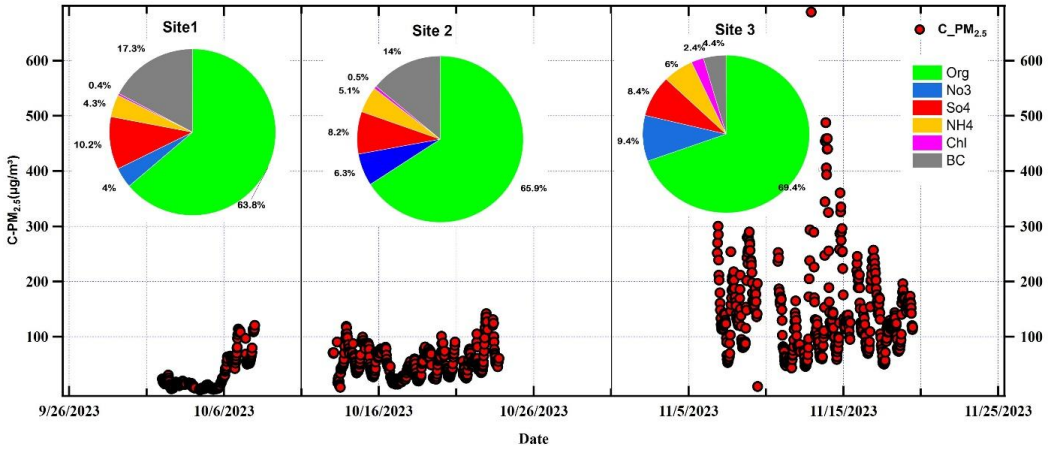

Figure.2: Time series of the C-$PM_{2.5}$ (µg/m^3) (NR-$PM_{2.5}$ +BC) with metals over Site1(CSIR -CIMAP), Site2 (BBAU) and Site3 (Talkatora) during the measurement period.

Figure.2 shows the temporal variation of C-$PM_{2.5}$ recorded during on-site air quality measurements by a VSAAQMP from October 2 to November 19, 2023, across three locations in Lucknow. The average $PM_{2.5}$ concentrations recorded during the campaign at Sites 1, 2, and 3 were 32.6 ± 33.8 µg/m^3, 58.31 ± 26.9 µg/m^3, and 227.20 ± 138.96 µg/m^3, respectively. The composition-based $PM_{2.5}$ estimate (C-$PM_{2.5}$), calculated as the sum of NR-$PM_{2.5}$, black carbon (BC),

https://doi.org/10.5194/egusphere-2026-595
Preprint. Discussion started: 13 March 2026

and metal components, was validated by correlating with reference-grade $PM_{2.5}$ measurements obtained from an EBAM ($PM_{2.5}$-EBAM) (Lakra et al., 2024).

Figure S1a-c shows the linear curve fitting between the C-$PM_{2.5}$ (NR-$PM_{2.5}$ + metals fraction of $PM_{2.5}$) and $PM_{2.5}$ -EBAM. We observed strong correlations between C-$PM_{2.5}$ and $PM_{2.5}$-EBAM (R^2 = 0.97 for Site 1, 0.86 for Site 2, and 0.90 for Site 3), indicating good agreement in the temporal variation of C-$PM_{2.5}$ with $PM_{2.5}$. The C-$PM_{2.5}$ mass was lower than the $PM_{2.5}$-EBAM values, likely due to the slight underestimation of NR-$PM_{2.5}$ by the AMS and the exclusion of metal oxides in Xact measurements, which report only elemental metals (Lalchandani et al., 2022). Further, the study indicates that Sites 1 and 2—representing background and traffic–residential environments—experience comparatively lower anthropogenic influence than Site 3(i.e., C-$PM_{2.5}$ about 7 times that of Site 1). The industrial activities at Site 3, combined with stagnant meteorological conditions (T = 22.1 °C, RH = 70.67%, and PBLH = 594.94 m), contribute to the enhanced concentrations of both organic and inorganic aerosols observed at this Site (Fig. S4b). In contrast, the relatively higher BC levels (~14%) at Site 1 are attributed to periodic wood and biomass burning associated with a lemongrass filtration process carried out for institutional research and commercial purposes (CSIR-CIMAP, 2025) (Fig. S10a). This activity, which occurred about 1.5km from the van, is also captured in our measurements during the last days of monitoring at Site 1 (6-7 October 2023), which are treated as the Polluted Day (PD) (Fig. S1ii). We have noted a significant concentration of OA (64%, 66%, and 70%) at all three Sites(Figure 2). This trend has also been observed at numerous locations throughout India and worldwide (Akanksha et al., 2025; Lalchandani et al., 2021; Shukla et al., 2025; Tsimpidi et al., 2024). Additionally, we observed concentrations of NO_3(4%,6%, and 9%), SO_4 (10%,8%, and 9%), NH_4 (4%,5%, and 6%), Chl(1%,1%, and 2%) and BC (17%,14%, and 4%) at Site 1, Site 2, and Site 3, respectively as shown in Figure 2. In the background Site 1 (post-monsoon), sulfate constitutes (~10%) a relatively larger share of the inorganic aerosol, and nitrate remains modest, consistent with a regional sulfate dominance, and a substantial fraction of nitric acid stays in the gas phase, limiting ammonium nitrate formation. At Site 2 (also post-monsoon), locally high NO_x and NH_3 emissions enhance ammonium nitrate formation compared with Site 1, but sulfate still represents an important sink for ammonia, so nitrate fractions are higher than at the background site yet remain below typical winter values. At Site 3 (winter), lower temperatures favor partitioning of nitric acid to the particle phase and, together with strong sulfuric-acid production from industrial/coal emissions, drive concurrent formation of ammonium sulfate and nitrate; this both increases total inorganic mass and elevates nitrate and sulfate fractions relative to the post-monsoon background and traffic Sites (Bhandari et al., 2020; Tsimpidi et al., 2024).

3.2 Source Apportionment of combined organic and inorganic aerosols

https://doi.org/10.5194/egusphere-2026-595
Preprint. Discussion started: 13 March 2026

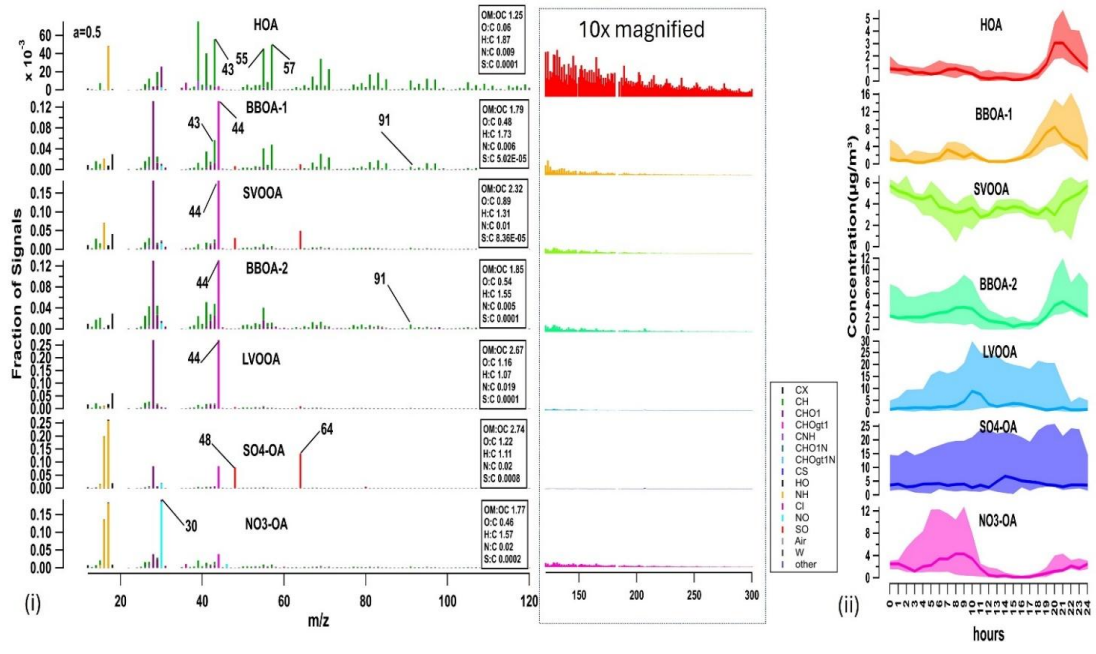

Figure 3. (i)Mass spectral profiles of sources/factors obtained from the combined Organics and Inorganics sources apportionment for m/z 12 to m/z 115, along with UMR spectra highlighted inside a grey border for m/z 120 to m/z 300. Elemental Ratios (O/C, OM/OC, H/C, and N/C) have been calculated using only the organic signals, and (ii)Diurnal variation of obtained sources during the measurement period over Site1.

The source factors were derived at three characteristically distinct sites in Lucknow. By applying a combined organic–inorganic Positive Matrix Factorization (PMF) approach, aerosol sources were resolved into primary and secondary organic components as well as inorganic species. Primary organic aerosols (POA) included hydrocarbon-like organic aerosol (HOA), representing traffic emissions, and biomass-burning organic aerosol (BBOA), indicating direct combustion sources. Solid fuel combustion (SFC) was identified as an additional primary organic marker, particularly evident at Site 3, and serves as an indicator of wood-burning activities. Secondary organic aerosols (SOA) were characterized by two OOA factors - low-volatile OOA (LVOOA) and semi-volatile OOA (SVOOA) representing oxidized organic-rich components derived from regional and urban photochemical processes. Inorganic-rich factors included sulfate-related organic aerosol (SO4-OA) and nitrate-related OA (NO3-OA), both formed via secondary oxidation and acid-base equilibria (Tsimpidi et al., 2024). The factor composition varied substantially across the three sampling Sites: Site 1 resolved two BBOA and one HOA factor alongside secondary OOA factors, reflecting mixed primary and secondary pollution; Site 2 was characterized predominantly by OOA factors with strong inorganic associations, indicating aged and processed aerosols; and Site 3 was dominated by the SFC factor, indicating solid fuel combustion as the primary pollution source during the sampling period. To gain insights into atmospheric composition from inter-site variation, we discuss these factors in the following sections.

3.2.1 Factor abundant in organic and inorganic compounds:

https://doi.org/10.5194/egusphere-2026-595
Preprint. Discussion started: 13 March 2026

3.2.1.1 HOA and SFC-OA: The mass spectra of HOA were predominantly composed of the hydrocarbon ion series of $C_nH^+_{2n-1}$ and CnH^+_{2n+1}, which characterizes the HOA spectrum. The $C_nH^+_{2n-1}$ includes m/z such as m/z 41(C_3H_5),55(C_4H_9),69(C_5H_9) as these are typical tracers of unsaturated hydrocarbon.The identification of alkane fragments (CnH_{2n+1}) at m/z 43 (C_3H_7+), 71 (C_5H_{11}+), and 98 (C_7H_{12}+), along with polycyclic aromatic hydrocarbon (PAH) fragments such as m/z 131, as traffic-related organic markers in aerosol mass spectrometry, is documented in several key references(Aiken et al., 2008; Lalchandani et al., 2022; Sun et al., 2012). The O: C ratio is observed to be nearly 0.05 at Site 1 and Site 2, which aligns with the values reported in a recent study over Lucknow (Lakra et al., 2024)(Figs. 3 and 4i–ii).Not only that, but worldwide studies have reported a lower O: C ratio of ~0.04 (Aiken et al., 2008; Sun et al., 2012). Additionally, the O:C ratio at Site 3 is 0.15, which may be attributed to a greater contribution from CHO groups (Fig.5i–ii). This indicates the secondary contributions, as indicated by the m/z signal, all C_xH_yO ions with $z > 1$ Figure. 3 (i). Moreover, the HOA factor is further confirmed by its strong correlation with NOx, with R values of 0.73, 0.83, and 0.48 (Fig. S8a-c). HOA levels from primary sources should be higher in the early morning or at night, as reported in earlier studies(Kumar et al., 2022; Lalchandani et al., 2021). Here, we have also observed bimodal peaks in the HOA variation during morning and nighttime hours. At Site 1, we have observed a very small variation in HOA, attributed to the lesser traffic influence. However, Site 2 experiences heavy traffic influence, resulting in significant observed variations. On the other hand, Site 3 exhibited greater variability, likely because its measurements were conducted during winter, when the PBLH is particularly shallow in the early morning and nighttime hours. We observed the highest HOA contribution in Site 3 (~6.9%), followed by Site 2 (~5.7%) and Site 1 (~3.5%)(Fig.6-8(ii)). Lower

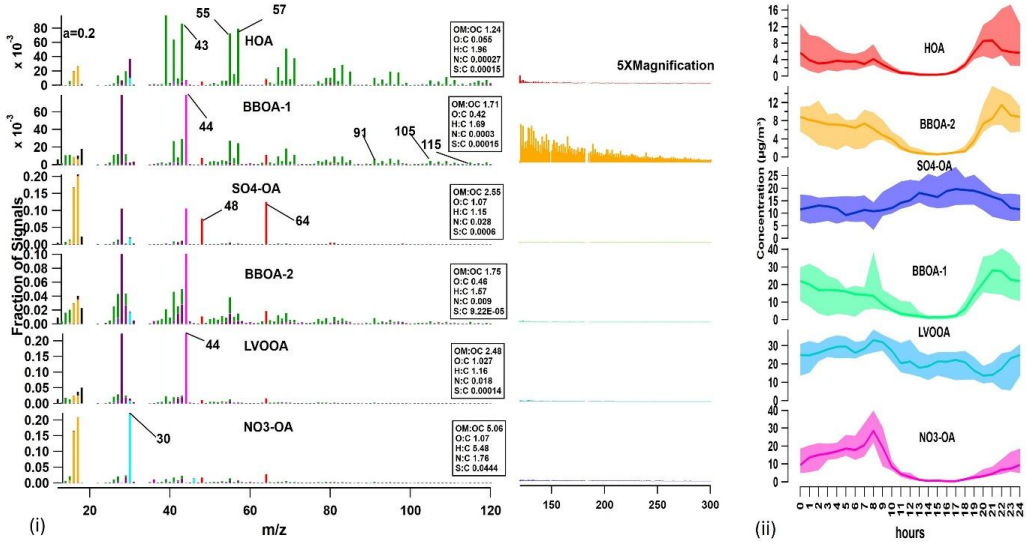

Figure 4. i)Mass spectral profiles of sources/factors obtained from the combined Organics and Inorganics sources apportionment for m/z 12 to m/z 115, along with UMR spectra highlighted inside a grey border for m/z 120 to m/z 300. Elemental ratios (O/C, OM/OC, H/C, and N/C) have been calculated using only the organic signals, and ii)Diurnal variation of the obtained sources during the measurement period over Site2.

https://doi.org/10.5194/egusphere-2026-595
Preprint. Discussion started: 13 March 2026

HOA at traffic-influenced Site 2 may result from higher PBLH and post-monsoon conditions, while elevated HOA at Site 3 likely stems from winter stagnation and lower PBLH(average ~594m) (Kumar et al., 2022).

The time-series variation of the HOA at site 1 shows smoother variation, indicating a lesser influence of traffic activity and a more urban background nature at site 1 (Fig. 6(i)). At Site 2, the HOA shows periodic variation, capturing daily traffic activity at the site; however, we observed a 30% decrease in HOA concentration within the university campus on every Wednesday, which, on 18th October 2023, was a no-diesel/petrol vehicle use day(Fig.7(i)). The time-series variation of the daily HOA values at site 3 shows higher variability, with a maximum value of 50 μg m^{-3} (Fig. 8(i)).

As far as the regional and local transport of these source factors is concerned, using the CWT, Figure. S9(i) panel (a) shows relatively low to moderate HOA source influence, with a narrow plume extending along the Indo-Gangetic Plain but weaker intensities near the receptor. This suggests that Site 1 is affected by more regional/transported traffic and combustion emissions rather than strong local HOA sources. Moreover, for Site 2, the CWT plot in Figure. S9(ii)(a) displays a more compact and intense HOA plume over north-central India, centered closer to the receptor point. The higher CWT values indicate stronger contributions from regional traffic/combustion corridors upwind of Site 2, consistent with its greater local traffic influence. On the other hand, Figure. S9(iii)(d) shows the strongest and most localized HOA concentrations, with high CWT values tightly concentrated around the receptor region. This implies dominant contributions from nearby traffic and combustion sources (e.g., roadside emissions at the downwind Talkatora location), making Site 3 the most impacted by HOA among the three Sites.

The SFC-OA factor exclusively resolved at Site 3 exhibits diagnostic m/z peaks: oxygenated fragments at m/z 29 (CHO^+), 39 ($C_3H_3^+$), 41 (C_2HO^+); unsaturated hydrocarbons at m/z 50 ($C_4H_2^+$), 51 ($C_4H_3^+$), 53 ($C_4H_5^+$); aromatic tracers at m/z 77 ($C_6H_5^+$), 91 ($C_7H_7^+$); high m/z PAHs at m/z 105, 107, 115, 128, 152, 165, 178, 189, 202; and nitrogen-containing organics at m/z 42 ($C_2H_4N^+$), m/z 45 (CH_3NO^+), m/z 71 ($C_3H_7NO^+$), m/z 73 ($C_3H_9NO^+$), reflecting incomplete combustion and NOx incorporation during solid fuel burning. We observed elevated SFC concentrations at night (20-23h), attributed to a shallow PBL with a mean height of ~266m and thus lesser vertical mixing during the night. The heat map confirms the SFC-OA shows a good Pearson coefficient, r = 0.77,0.78, and 0.98 with m/z 77,91, and 115, respectively (Fig. S8c), which are the key tracers for incomplete combustion at Site 3 (Lakra et al., 2024; Mohr et al., 2012) (Fig. S8c). The strong relationship between key tracers and SFC-OA confirms that the source factor is primarily linked to solid-fuel combustion. Moreover, the diurnal correlation of SFC-OA with BC (r = 0.39) further indicates the contribution of SFC-OA from solid fuel combustion activities near Site 3 (Fig. 5(i)). We have observed that the SFC-OA contribution accounts for about 10% of all OA-resolved factors at Site 3 (Fig.8(ii)). The diurnal profiles of CO and SFC-OA show a strong correlation (r = 0.91), supporting their shared origin from incomplete combustion processes (Tong et al., 2021). We also observed a quite high Pearson correlation of 0.51 between RH and SFC. High RH enhances SFC-OA by driving semi-volatile combustion products into the particle phase and promoting aqueous/heterogeneous processing on wet aerosols (Tobler et al., 2021). Under shallow, humid boundary-layer conditions (e.g., winter nights and early mornings), when domestic heating and biomass burning are more prevalent, and dispersion is limited, this results in elevated SFC-OA (Tong et al., 2021). The time-series variation of the SFC-OA shows a peak whenever there is solid-fuel combustion activity near the site during the measurement

https://doi.org/10.5194/egusphere-2026-595
Preprint. Discussion started: 13 March 2026

period(Fig.8(ii)). The CWT plot for the SVOOA (Fig.S9(iii)) shows the major contribution with concentrations 10-16µgm^{-3} from local activities near Site 3.

3.2.1.2 LVOOA:

In AMS source apportionment, Low-volatile-OOA (LVOOA) is an aged, highly oxidized SOA factor, typically interpreted as regionally transported or long-aged OA rather than fresh local emissions. LVOOA is characterized by a dominant peak at m/z 44 (CO_2^+), often accompanied by prominent peaks at m/z 28 (CO^+) and 18 (H_2O^+), reflecting high oxidation. Higher O: C and oxidation state than SV-OOA and primary factors (HOA, SFC-OA, BBOA), which vary between 1.02 and 1.16 across the three Sites, indicating its highly oxidized or aged nature (Fig.3-d). We observed that LV-OOA accounted for 24.0%, 31.6%, and 17.9% of the total organic and inorganic aerosol at Sites 1, 2, and 3, respectively (Fig.6-8(ii)). Our findings at the urban Sites are in line with concentrations reported in urban European cities, which have shown that LVOOA commonly contributes ~30-40% of OA (Canonaco et al., 2015; Reyes-villegas et al., 2016).

At Site 1, we have observed a flat diurnal profile compared to Sites 2 and 3, with only a modest afternoon increase, reflecting photochemical production and mixing, and thus an aged LVOOA contribution(Kumar et al., 2022). The diurnal profile at Site 1 shows that LVOOA concentrations remain elevated from 10:00 to 19:00, indicating SOA formation through photochemical oxidation during daytime hours (Fig. 3 (i)). The lesser variation we observed for the larger daytime span (10:00-19:00 hours) at Site 1, with nearly 50% lower concentration, suggests that it is of a background nature. During the night hours, a fall after a small rise in the LVOOA over Site 1 was observed; on the other hand, a rise in the LVOOA occurred after a dip in concentration at 20:00 hours at Sites 2 and 3, respectively. At night, it is common to see LVOOA decrease at cleaner/background Sites and increase at traffic/industry Sites, because nighttime chemistry and boundary-layer dynamics favor local primary and semi-volatile emissions in polluted areas, while cleaner Sites mainly see regional background (Lalchandani et al., 2021; Liu et al., 2024b).

The time series variation of the LVOOA shows the smooth variation with almost 50% lesser concentration as compared to the Sites 2 and 3, respectively (Fig.6-8(ii)).

At Site 1, LVOOA's r = 0.41 with NO_3 (vs. 0.22 with SO_4) arises from shared nocturnal partitioning, nitrate radical oxidation, and regional ammonium nitrate transport dominating over stable sulfate in post-monsoon conditions (Bhandari et al., 2020) (Fig. S8a).

The NO_3 drives LVOOA via nighttime NO_3 radical reactions on VOCs (common in urban backgrounds), yielding a higher r=0.41 despite regional origins. The SO_4's weaker r = 0.22 reflects the decoupling of its aqueous-phase formation from LVOOA's gas-phase oxidation steps. This pattern reflects nitrate's semi-volatility, aligning with LVOOA formation, while sulfate's regional aqueous processing decouples temporally. A similar nitrate preference in oxygenated OA is observed in Delhi PMF studies (Bhandari et al., 2020; Cash et al., 2021). This was further confirmed by the CWT of LVOOA for Site 1, as a good relation with nitrate might be due to IGP transport of nitrate-rich plumes. In line with the above, we observed a weaker

https://doi.org/10.5194/egusphere-2026-595
Preprint. Discussion started: 13 March 2026

correlation with sulfate at Site 2 (R = 0.30). However, at Site 2, a higher LVOOA–nitrate (R=0.54) than LVOOA–sulfate (R=0.30) correlation implies that LVOOA variability is more closely linked to local/near-regional nitrate formation than at the background Site 1 (Fig. S8a). At Site 3, weaker correlations with both sulfate and nitrate (R=0.37 and 0.25) suggest a more heterogeneous mixture of industrial plumes and regional background, which reduces the simple LVOOA–sulfate coupling seen at the background Site (Fig. S8(b-c)) (Hao et al., 2014). Furthermore, the above pattern aligns with the CWT spatial pattern, in which Site 1 receives contributions from long-range transport from Punjab and Haryana during the biomass burning period (Fig.S9(i) and (e)). The Site 2, LVOOA concentration gradient is more local to the Site 2 (Fig. S9(ii),c). Moreover, at Site 3, LVOAA concentration contributed more from both local and distant sources (Fig. S9(ii) (g)).

3.2.2.3 SVOOA:

The less oxidized SVOOA (semi-volatile oxygenated organic aerosol), typically characterized by higher f_{43} (m/z 43, $C_2H_3O^+$) and lower f_{44} (m/z 44, CO_2^+) signals relative to LVOOA represent fresher SOA in standard classifications. However, our hyperlocal Sites 1 and 3 show the reverse—$f_{44} > f_{43}$—indicating relatively aged SVOOA despite its semi-volatile nature (Fig. 3i, iii)(Sun et al., 2012), with Site 3 exhibiting a particularly prominent $(CHO_1)^+$ group at m/z 44 as a classic aging marker. PMF analysis resolved SVOOA exclusively at Sites 1 (10.1% of OA) and 3 (18.6% of OA)(Fig.6 and 8 (ii)), aligning with background values (15–35% of OA) and urban environments (~20–40% of OA)(Budisulistiorini et al., 2016; Minguillón et al., 2015; Ripoll et al., 2015; Xu et al., 2019) Site 1 showed a higher O: C ratio (0.89 vs. 0.58 at Site 3). This pattern mirrors Barcelona's SV-OOA, featuring high f_{44} from carboxylic acids alongside hydrocarbon fragments (m/z 29, 43, 55, 57)(Mohr et al., 2012; Zhang et al., 2014). Moreover, in some ambient and chamber cases, spectra of fresher SOA or SV-OOA already show a strong m/z 44 peak due to carboxylic acids. They can show f_{44} comparable to or larger than f_{43}, while still being clearly less oxidized than LV-OOA in O: C and overall pattern(Canonaco et al., 2015; Zhang et al., 2014).

SVOOA at Site 1 exhibits multimodal variation dominated by nighttime peaks. The strong midnight maximum reflects efficient NO_3/O_3-driven and aqueous-phase SOA formation under humid (~80%) conditions and shallow boundary layer (~324 m)(Gu et al., 2023). A weaker afternoon peak indicates diluted daytime photochemistry, while a fairly flat overall variation suggests the presence of aged SVOOA. At Site 1, SVOOA shows much lower daily temporal variability throughout the measurement period (Fig. 6 (i)). Moreover, at Site 3, the elevated values range from 10 to 80 μg m^{-3}. As time progresses, the variation becomes smoother (Fig. 8(i)).In contrast, Site 3 shows bimodal variation with a primary peak between 9:00 and 10:00 h. This daytime maximum is linked to active photochemical oxidation, boundary-layer rise, and nearby combustion (Gu et al., 2023; Kuang et al., 2020). A secondary late-afternoon peak arises from limited winter photochemistry.

Site 1 demonstrates nighttime dominance of nitrate over aqueous species. Site 3 reflects daytime photochemistry control, consistent with central IGP winter studies(Lakra et al., 2024). Supporting correlations include strong NO_3 (r = 0.83 vs. 0.52), moderate NH_4^+ (r = 0.20-0.31), and weak SO_4 linkage. SVOOA typically couples to fresh traffic/anthropogenic SOA via NOx chemistry. At a clean Site 1, aging processes transform POA into SVOOA, leading

https://doi.org/10.5194/egusphere-2026-595
Preprint. Discussion started: 13 March 2026

to an increase in organic nitrate fractions, while inorganic nitrate and sulfate levels may decline due to volatilization or limited precursor availability (Wu et al., 2024). Another reason could be differences in volatility in the clean environment; inorganic nitrate is more volatile and tends to evaporate under warmer conditions. Site 1 has the highest temperature among all Sites, at ~29.6 °C during the sampling period. Therefore, it reduces its particle-phase concentration (Matsumoto and Tanaka, 1996; Zhang and McMurry, 1992). The above-mentioned SVOOA reason for Sites 1 and 3 was also confirmed by the CWT plots, which explained their different origins.

The CWT plots (Fig. S9i (f–g) and c) reveal long-range transport of SVOOA from northern India to Site 1, enhanced by high temperatures (~29.6°C) volatilizing inorganic nitrate/sulfate, while aging promotes organic nitrates, versus steady traffic/industry formation at Site 3 under stagnant winter conditions (Fig. S9iii (a)). In line with our observation at Site1, the studies reported that overclean sites often originate from biogenic VOCs oxidized by nitrate radicals, producing organic nitrates and semi-volatile organics that do not necessarily co-occur with inorganic nitrates and sulfates, which are more anthropogenic or long-range transported (Fry et al., 2014; Song et al., 2024).

3.2.2.4 BBOA-1 ,BBOA-2 and O-BBOA

BBOA was resolved into three related factors, each with characteristics that vary across the three Sites(Lakra et al., 2024). At Site 1, BBOA-1 represents fresh, less oxidized biomass-burning emissions, with relatively low signal at m/z 43 and 44 but enhanced high-m/z (>120) fragments characteristic of PAHs and incomplete combustion (Fig. 3), and strong anhydrous fragments at m/z 60 and 73 indicating levoglucosan-like tracers(Daellenbach et al., 2017). Its O: C ratio (≈0.48) is lower than that of the more aged BBOA-2, (Florou et al., 2017) and it contributes about 10.1% of OA(Fig.6(ii)), showing a clear early-morning peak (07:00–08:00)(Fig.S3 g) linked to residential wood/coal use, agricultural burning, and trapping in a shallow boundary layer(Zhang et al., 2015). Its correlation with nitrate is weak (r = 0.19), consistent with decoupled primary biomass-burning emissions (Fig. S8a). BBOA-2 at Site 1 is more oxidized (O: C ≈0.54), with enhanced m/z 43 and 44 and much lower PAH intensities, contributes about 12.9% of OA(Fig.6(ii)), peaks 1–2 hours after BBOA-1 (around 09:00–10:00), and correlates strongly with nitrate (r ≈0.69), implying rapid oxidation of fresh BBOA-1 (Fig. S8a) and stronger association with nitrate-related chemistry and organonitrates(Kaltsonoudis et al., 2025). The time-series variation of BBOA-1 shows greater daily variability than that of BBOA-2, which has much less (Fig. 6(i)). These variations depict the aged nature of BBOA-2. CWT analysis indicates that both BBOA-1 and BBOA-2 at Site 1 are influenced by regional biomass burning across the IGP, particularly post-monsoon agricultural burning in Punjab and Haryana (Fig. S9.(i))(Lalchandani et al., 2022), with additional contributions from local open burning and lemongrass filtration activity.

At Site 2, a traffic-influenced urban location, BBOA-1 again represents fresh biomass-burning OA with spectral features similar to Site 1 but a slightly lower O: C (≈0.42), indicating even less oxidation; it contributes a larger fraction (≈20.1% of OA)(Fig.7(ii)), and its morning peak (07:00–08:00) reflects proximity to fresh emissions from waste burning, residential cooking, and open biomass burning near the roadway(Fig. S3.g). Its correlation with nitrate remains weak (r ≈0.26), reinforcing its characterization as a primarily primary, non-nitrate-coupled biomass-burning factor(Fig. S8b). BBOA-2 at Site 2 is the aged counterpart, with higher m/z 43 and 44 and low PAH signals, an O: C

https://doi.org/10.5194/egusphere-2026-595
Preprint. Discussion started: 13 March 2026

of ≈0.46, and a more minor OA contribution (≈7.7%) than BBOA-1; it peaks about 1–2 hours after BBOA-1, consistent with rapid oxidation, and shows a stronger correlation with nitrate (r ≈0.41), pointing to enhanced connections with nitrate and organonitrate chemistry(Zheng et al., 2020). In contrast to Site 1, BBOA-1 shows more variability with concentration at Site 2 (Fig.7(i)).CWT results for BBOA-1 at Site 2 show an elongated plume along the IGP with a hotspot near the receptor (Fig. S9.(ii)), indicating a combination of regional biomass-burning transport and strong local sources.

At Site 3, a highly polluted industrial environment, biomass-burning OA is dominated by an oxidized BBOA factor (O-BBOA). O-BBOA shares biomass-burning tracers such as m/z 60 and 73 but has very low high-m/z (>120) PAH intensities, indicating substantially aged biomass-burning aerosol(Fig.5i). Its O:C ratio (≈0.48) is comparable to BBOA-1 at Site 1 but lower than values reported at other CIGP Sites, such as Kanpur and Lucknow(Lakra et al., 2024), and it contributes about 20% of OA(Fig.8(ii)). O-BBOA shows a low correlation with nitrate (r ≈0.03) and only a weak association with the biomass-burning marker m/z 60 (r ≈0.24), both consistent with a more aged biomass-burning plume whose variability is decoupled from contemporaneous nitrate formation. Diurnally, O-BBOA exhibits relatively high morning concentrations, exceeding those at the other two Sites (Fig. 5ii), and a very strong nighttime enhancement in winter, with nighttime levels about three times those during the day (Fig. S3h). This behavior likely reflects NO_3 radical-driven oxidation of fresh biomass burning emissions, combined with a shallow, stable nocturnal boundary layer that traps combustion products and high relative humidity (~71%) that promotes the partitioning of semi-volatile biomass burning products and aqueous/heterogeneous oxidation (Lhotka et al., 2025). The strong correlations of O-BBOA with CO, NOx, SO_2, and BC (r > 0.6) further indicate its close linkage to combustion sources under humid, stagnant conditions (Awasthi et al., 2024). The time-series variation of the O-BBOA shows greater variation between 8-17 October 2023; thereafter, we observed lesser variation approaching the extreme winter conditions (Fig. 8(i)).

The CWT results indicate a broad source region extending from north-central to eastern IGP, with a dominant air mass influence from Punjab and Haryana, likely linked to post-monsoon agricultural stubble burning in these areas for Site 1 (Fig. S9(i)). The map for Site 2 shows the potential source regions that influence the BBOA-1 factor (Fig. S9(ii)). The elongated plume from northwest to southeast, with a hotspot near the receptor, indicates that BBOA-1 is mainly associated with regional biomass burning upwind of the IGP, with moderate–strong contributions reaching the Site 2.CWT analysis of the O-BBOA-dominated factor at Site 3 reveals a compact, intense hotspot over northern India (Fig. S9. (iii)), highlighting a strong local and near-regional biomass-burning influence around the receptor, consistent with elevated nighttime O-BBOA and nearby residential and solid-fuel burning.

Across the three Sites, BBOA-1 captures fresh biomass-burning emissions, BBOA-2 represents more aged biomass-burning OA with stronger nitrate coupling at Sites 1–2, and O-BBOA at Site 3 characterizes aged, highly polluted biomass-burning aerosol that accumulates under humid, stagnant winter conditions. Site-wise differences in O:C ratios, contributions, correlations with NO_3^- and tracers, and diurnal cycles together indicate a transition from regionally influenced biomass burning at the background Site, through locally amplified emissions at the Site 3, to strongly aged and trapped biomass-burning aerosol at the industrial, highly polluted Site.

https://doi.org/10.5194/egusphere-2026-595
Preprint. Discussion started: 13 March 2026

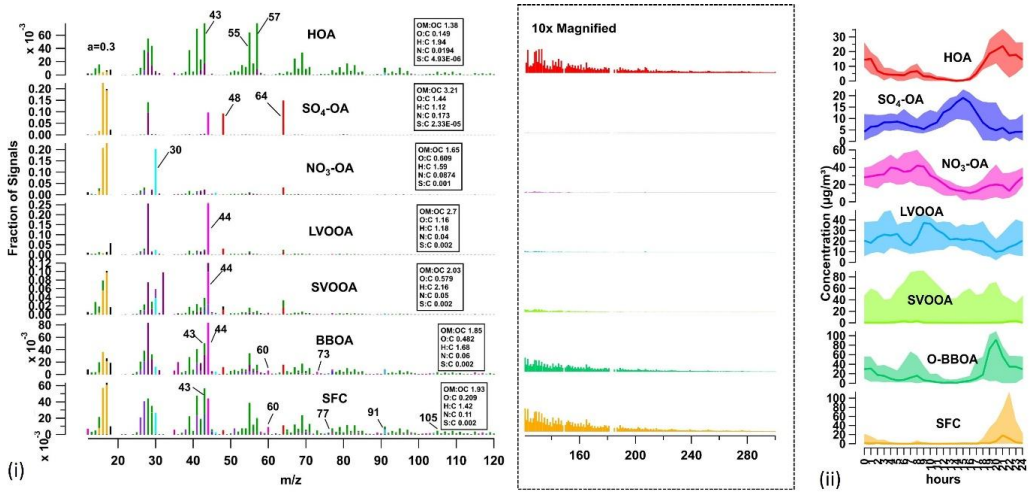

Figure 5. i)Mass spectral profiles of sources/factors obtained from the combined Organics and Inorganics sources apportionment for m/z 12 to m/z 115, along with UMR spectra highlighted inside a grey border for m/z 120 to m/z 300. Elemental Ratio(O/C, OM/OC, H/C, and N/C) has been calculated using only the organic signals, and ii)Diurnal variation of obtained sources during the measurement period over Site3.

3.2.2.5 NO_3-OA and SO_4-OA: The NO_3-OA and SO_4-OA factors together represent the secondary inorganic aerosol (SIA) component. The SO_4-OA, a major inorganic-rich factor, exhibited higher intensity of sulfate ions at m/z 64 (SO_2), m/z 48 (SO), and ammonium ions at m/z (NH_3) and m/z 16 (NH_2) in its mass spectra (Fig. 3-5) at all Sites. It primarily consisted of ammonium sulfate, with ~68%, 59%, and 68% of the total mass of this factor. Followed by the organics contributed, 29%, 39%, and 32%, with O/C ratios among all factors (1.22, 1.07, 1.07, and 1.44) in Site 1, Site 2, and Site 3, respectively (Fig. 6-8(i)). The highest O/C ratio indicates a highly oxidized nature of the organics within the factor. The SO_4-OA shows correlations (r = 0.98, 0.68, and 0.61) with sulfate from AMS and sulfur from the metal monitor (r = 0.72) across three Sites (Fig. S9 and S2). The very high correlations of SO_4-OA with AMS sulfate at all three Sites (r = 0.98, 0.68, 0.61) and with sulfur from the metal monitor (r = 0.72) indicate that this factor is tightly linked to sulfate-rich aerosol and sulfur-containing emissions (Saarikoski et al., 2019). This implies that SO_4-OA predominantly represents secondary sulfate-associated organic aerosol formed in or on sulfate particles (e.g., via multiphase oxidation of SO_2 and organics), and that the same sulfur sources and formation pathways (industrial/coal SO_2, regional sulfate production) control both the inorganic sulfate and the associated SO_4-OA factor (Xu et al., 2016). The time-series variation of SO_4-OA shows very low variability (~4-5 times less) at site 1 compared to sites 2 and 3 (Fig. 6-8(i)).

All the secondary inorganic components show a prominent peak at ~9-10 am, coinciding with NO_X (r=0.85) at Site1(Fig. S4a and S2). NOx peaks align with NO_3-OA and SO_4-OA because NOx is a key precursor for both nitrate and sulfate formation. Elevated NOx promotes production of nitric acid (driving particulate nitrate) and enhances multiphase oxidation of SO_2 to sulfate, so secondary inorganic aerosol and NOx rise together in the late morning (Squizzato et al., 2013). The NO_X morning peak during the traffic rush hours and onset of mixing (PBLH) increases

https://doi.org/10.5194/egusphere-2026-595
Preprint. Discussion started: 13 March 2026

from ~200m at 9:00 to 11:00 over 1 km (Fig. S4a and g). The SO_4-OA shows a strong correlation with ozone (O_3) at Site 1, with r = 0.62 (Fig. S9 and S4d). The strong correlation between SO_4-OA and O_3 suggests that sulfate-related OA forms under photochemically active, oxidizing conditions where ozone is abundant. Elevated O_3 reflects intense daytime photochemistry and high oxidant levels, which enhance multiphase oxidation of SO_2 to sulfate (one of the main pathways involves O_3 as an aqueous oxidant), so periods with more O_3 naturally coincide with greater sulfate and associated SO_4-OA production. The SO_4-OA formation insights are further obtained by estimating the sulfur oxidation ratio (SOR) for all three Sites (Fig. S5) (Lakra et al., 2024). SOR was estimated to be higher at the highly polluted Site 3 than at the moderately polluted Site 2 and the less polluted Site 1 (Fig. S5). The range of SOR values at Sites 1 and 2 was approximately half that observed at the highly polluted Site 3 (Fig. S5). Both SOR and SO_4-OA (see Fig.S5 and 6d) increase between 9:00 and 19:00 hours, indicating photochemical production of SO_4-OA under conditions of high temperature and low relative humidity. Additionally, the SOR values at Sites 3 and 2 showed minimal variation, suggesting that both aqueous-phase and photochemical processes contribute significantly to sulphate formation at Site 3 (Lalchandani et al., 2022; Sun et al., 2012).

The CWT analysis for site 1 indicates that the SO_4-OA factor predominantly contributes at low concentrations (2–3 μgm^{-3}), with primary transport from the northwest region of the Uttar Pradesh district (Fig. S9i-c). At sites 2 and 3, regional advection from Punjab and Haryana governs contributions in the 10–15 μgm^{-3} range (Fig. S9ii-c) and 15–25 μgm^{-3} range (Fig. S9iii-b), respectively. Regional transport concentrations exhibit a marked seasonal escalation from post-monsoon to winter, consistent with enhanced secondary sulfate formation under stagnant meteorological conditions.

At all three Sites, the NO_3-OA factor was predominantly ammonium nitrate, accounting for approximately 52%, 62%, and 66% at each Site, respectively (Fig. 3–5). The mass spectra for this factor, displayed in Figures 3–5, show high-intensity peaks at m/z 46 (NO_2) and m/z 30 (NO).

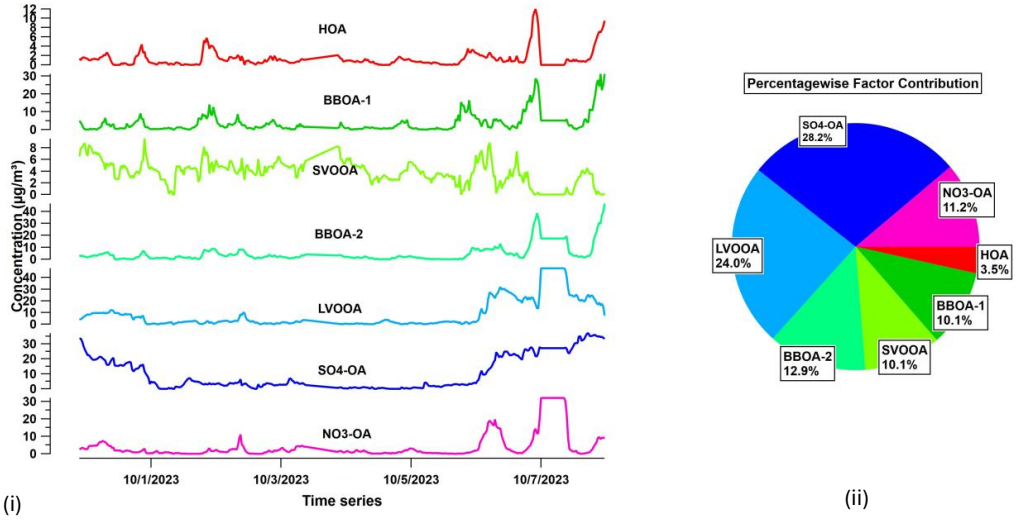

https://doi.org/10.5194/egusphere-2026-595
Preprint. Discussion started: 13 March 2026

Figure 6. i)Time series variation of the NR-$PM_{2.5}$ sources obtained from combined OA and Inorganics sources apportionment ii) Average chemical composition of NR-$PM_{2.5}$ composition during the measurement period over Site 1.

Furthermore, the Nitrogen Oxidation Ratio (NOR), an indicator of secondary NO_3-OA formation, was high during the nighttime and early morning, peaking around 05:00. NOR values were consistently higher at the more polluted sites (Fig. S5). In addition, both SOR and NOR in this study were substantially higher than those reported in previous winter campaigns (2021–2023) at CIGP Sites, such as Lucknow and Kanpur, indicating a higher degree of SOA formation under more polluted conditions (Lakra et al., 2024). During the post-monsoon to winter period in Lucknow and Kanpur, levels are higher than those reported in previous winter campaigns, likely due to enhanced atmospheric oxidation capacity and changing emission or meteorological conditions (Chang et al., 2022; Wang et al., 2024).

The time-series variation of NO_3-OA is too smooth, except at the last observation period on the polluted event day, compared with Sites 2 and 3 (Fig. 6-8(i)). This might be due to the regional build-up contribution only at Site 1.

The diurnal profile reveals that the peak of NO_3-OA occurred approximately two hours after the morning peak of HOA at Site 1, and about one hour later at Site 3(Fig.6c and h). Morning rush-hour traffic emits primary HOA and NOx first, peaking under a shallow boundary layer. The rising sun then drives NOx oxidation to particulate nitrate (1–2 h timescale) and its mixing into NO_3-OA, causing the delayed peak (Chen et al., 2021; Poulain et al., 2011). In contrast, at Site 2, which is characterized by both traffic and residential influences, HOA and NO_3-OA peaked simultaneously during the morning hours (Fig. S3e and c). This pattern suggests that ammonium nitrate formation results from the reaction between NO_x (emitted from traffic) and ammonia, facilitated by the gas-phase oxidation of NO_x by OH radicals under conditions of low ambient temperature (~20.5ºC) and high RH (90%) (see Fig. S4e and S4f). Following these peaks, concentrations decrease rapidly throughout the day as rising temperatures promote the conversion of nitrate particles to nitric acid and ammonia ($NH_4NO_3 \rightarrow HNO_3 + NH_3$), consistent with findings from previous studies (Faisal et al., 2022; Lakra et al., 2024; Sun et al., 2012). The concentration further increases at night, primarily driven by nighttime chemistry in which NO_x is oxidized by ozone at higher altitudes through heterogeneous reactions (Wang et al., 2018; Yun et al., 2018). This process occurs under conditions of high relative humidity (RH > 92.16% at Site 1, RH > 86.23% at Site 2, and RH > 82.66% at Site 3) and low temperatures (AT <25.8°C at Site 1, < 21.3°C at Site 2, and < 19.0°C at Site 3), Such conditions facilitate the formation of these compounds in the upper tropospheric layers across all three Sites (Chang et al., 2011). This process was further validated by strong nighttime correlations between NOR and NO_3-OA, with coefficients of 0.92, 0.96, and 0.97 at the three Sites (Fig. S3.6c and S5b). These high correlation values provide additional evidence for the concentration increase at both Sites, supporting the role of heterogeneous reactions. In contrast, rising ambient temperature (AT) during the afternoon is associated with a decrease in concentration.

The CWT analysis shows that NO_3-OA mainly contributes at 2-3.5 μgm^{-3} at site 1, located northwest of Site 1 (Fig. S9i-c). Sites 2 and 3 show major local contribution from northwesterly wind transport of 2-8 μgm^{-3} (Fig. S9ii-d) and 15-30 μgm^{-3} (Fig. S9iii-f), respectively. The local transport concentrations increase progressively from post-monsoon to winter, reflecting enhanced secondary nitrate formation under stagnant conditions.

https://doi.org/10.5194/egusphere-2026-595
Preprint. Discussion started: 13 March 2026

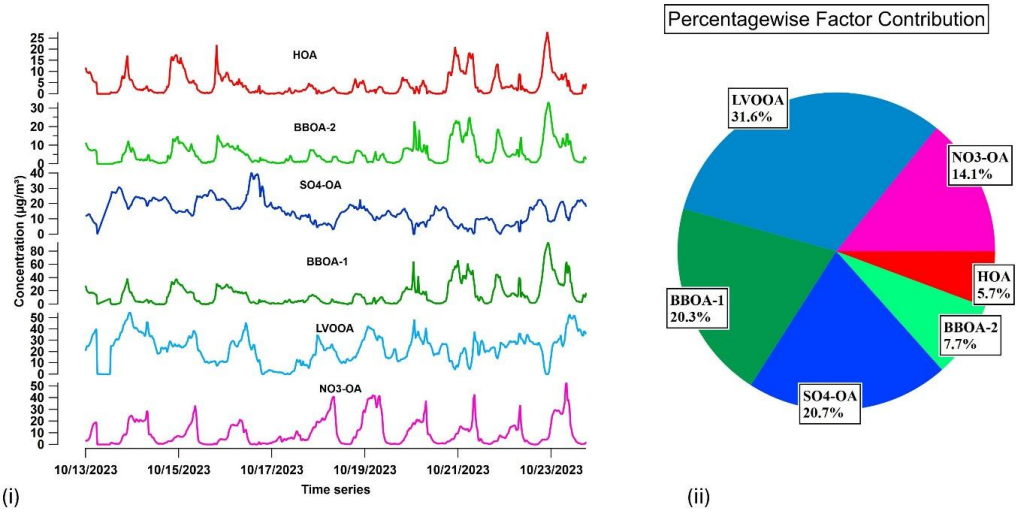

675

676 **Figure 7. i)Time series variation of the NR-$PM_{2.5}$ sources obtained from the combined OA and IOA sources apportionment.**
677 **ii) Average chemical composition of NR-$PM_{2.5}$ during the measurement period over Site 2.**

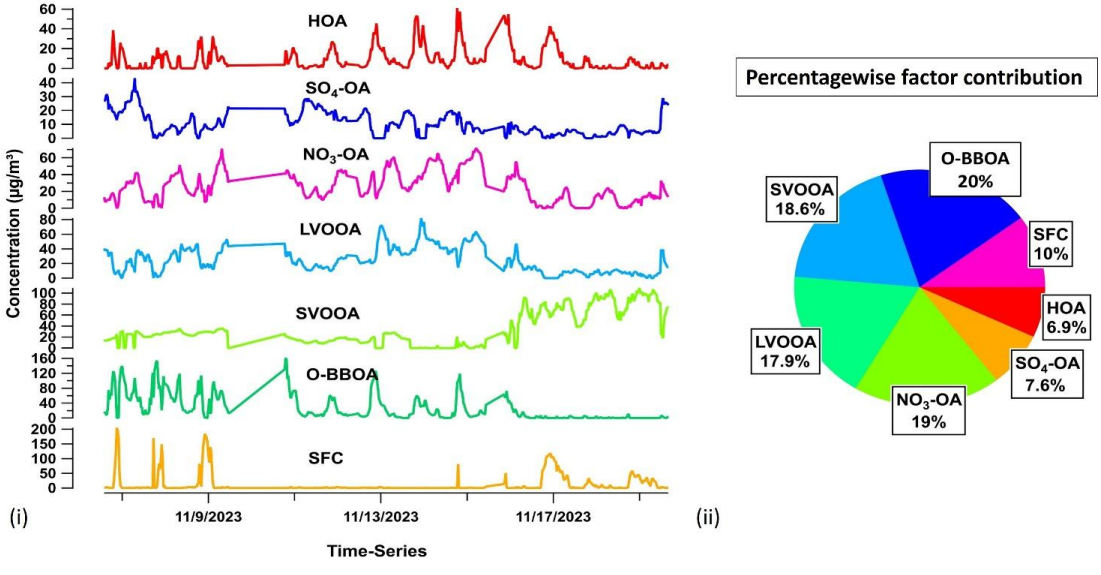

678

679 **Figure 8. i)Time series variation of the NR-$PM_{2.5}$ sources obtained from combined OA and IOA sources apportionment ii)**
680 **Average chemical composition of NR-$PM_{2.5}$ during the measurement period over Site 3.**

681

https://doi.org/10.5194/egusphere-2026-595
Preprint. Discussion started: 13 March 2026

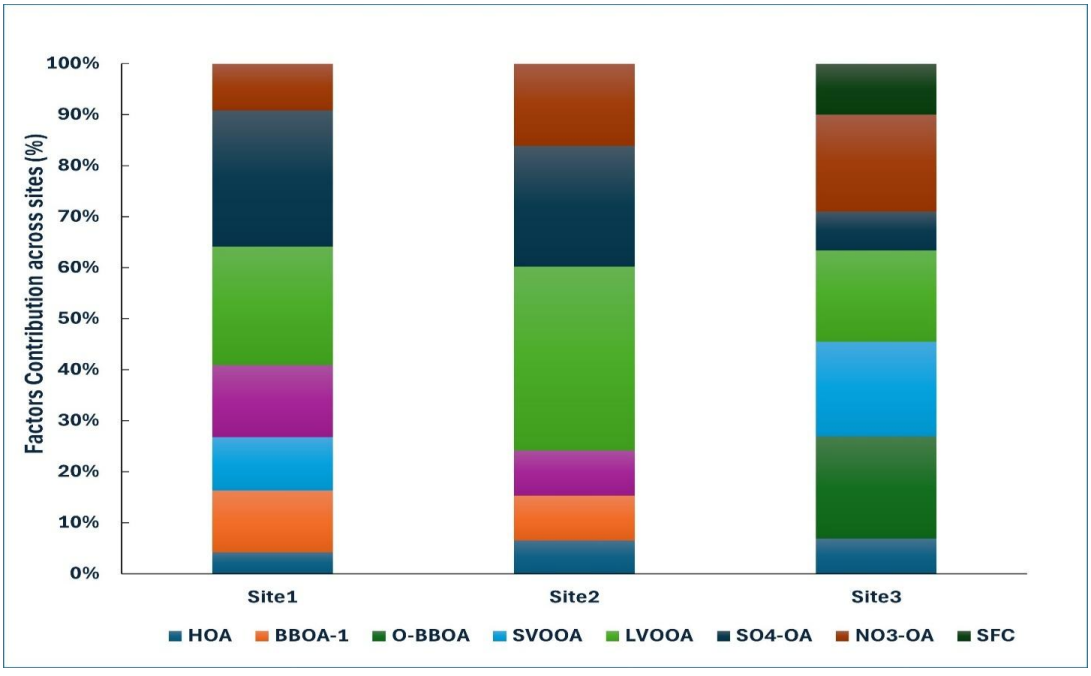

Figure 9. Factor abundant contribution across all three measurement Sites.

3.3 Local and Regional contribution in three Sites

Previous research has demonstrated that source apportionment factors are valuable for distinguishing and quantifying the contributions of local and regional aerosol transport within a given area (Jimenez et al., 2009; Sun et al., 2011; Zhang et al., 2007). Specifically, the combined presence of LVOOA and SO_4-OA typically indicates regional transport. In contrast, SVOOA and NO_3-OA are primarily linked to the oxidation of local emissions at a Site. Figures 9 and 10 show the factors contributing to each Site, as well as long-range and local transport at all three Sites during the measurement period. Regional transport dominated at Sites 1 and 2, contributing 52.6% and 52.3%, respectively, but only 25.3% at Site 3 (Fig.10). Conversely, local sources accounted for 74.7% at Site 3, compared to 47.4% at Site 1 and 47.7% at Site 2 (Fig.10). The reason for this contribution might be that the transboundary emissions from neighboring states account for 70-80% of $PM_{2.5}$ in Lucknow, carried by prevailing winds, stubble burning, industrial sources, and vehicular traffic, which overwhelms local contributions even at Sites 1 and 2, respectively(The Energy and Resources Institute, 2022).

https://doi.org/10.5194/egusphere-2026-595
Preprint. Discussion started: 13 March 2026

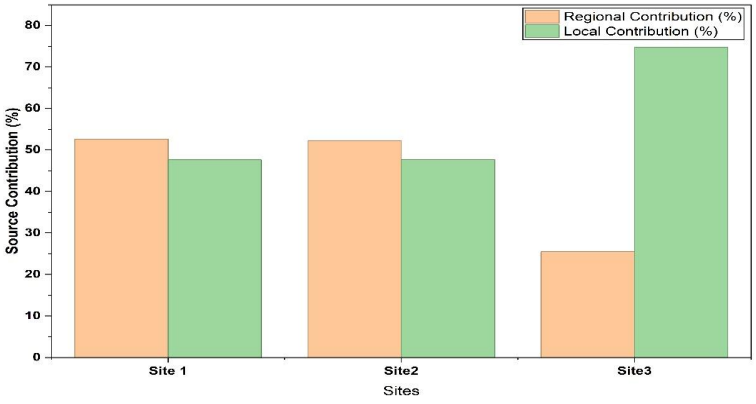

Figure 10. Source contribution across different Sites during the measurement period.

This regional influence is clearly reflected in the concentration-weighted trajectory plots, which show that transboundary emissions transported by prevailing winds from neighboring states constitute a major share of $PM_{2.5}$ sources in Lucknow (Fig. S9i–iii). Notably, there was a significant contribution from the northwestern direction, particularly from the northern IGP regions of Punjab and Haryana. Figures S9(i)e and S9(i)g clearly demonstrate the long-range transport of aged LVOOA and NO_3-OA particles from neighboring states and countries over Site 1. Similarly, at Site 2, we observed a notable influence of regional transport, likely due to comparable meteorological conditions and prevailing wind patterns, as all measurements were conducted during the same season. Additionally, concentrations of LVOOA and SO_4-OA were considerably higher at Site 2 (Fig. S9(ii)). Given Site 2's proximity to a highway or high-traffic area, Figure S9(ii, b) shows a notable contribution of HOA from nearby sources. In contrast, at the highly polluted Site 3, we detected a significant local contribution, with elevated levels of BBOA, HOA, SFC, NO_3-OA, and SVOOA observed in close proximity to the Site (Fig. S9(iii)).

3.4 Case study of the PGE

PGEs are defined as periods during which particle number concentration increases, accompanied by a shift in the mode toward larger geometric diameters, typically following new particle formation (Zimmerman et al., 2020). This growth is driven by condensation of low-volatility vapors (such as sulfuric acid and organic compounds) onto freshly nucleated clusters, leading to a relative decrease in the organic mass fraction compared to inorganic components in the growing mode (Tröstl et al., 2016). In the present study, PGEs are selected under conditions where the CS exceeds 0.1 s^{-1}, indicating a relatively high background aerosol loading that efficiently scavenges condensable vapors. Here, we will discuss the PGEs that we observed at Site 1 during the campaign (Fig. S7(i)). We observed the two particle growth events, PGE 1 and 2, respectively. The estimated particle growth rates are 2.68nm/hr. and 4.82nm/hr., respectively. During the measurement period at Site 2, five PGE events were recorded (Fig. S7 (ii) and Table 1). Four of these events exhibited growth rates between 1.12 and 1.59 nm/hr, except for October 20, 2023, when an elevated growth rate of approximately 6.15 nm/hr was observed. The van, stationed within the university campus area

https://doi.org/10.5194/egusphere-2026-595
Preprint. Discussion started: 13 March 2026

surrounded by vegetation and shrubs, showed comparatively lower growth rates. At Site 3, we detected 10 such events, with growth rates ranging from 4.97 to 16.51 nm/hr (Fig. S7(iii) and Table 1). Despite this high sink, sustained growth is observed, suggesting that local vapor sources (e.g., from traffic, cooking, or secondary formation) are sufficient to support continued particle growth even in a polluted urban environment. We observed higher particle growth rates in polluted environments and lower growth rates in cleaner environments, consistent with previously reported data for similar conditions over the northern IGP (Mishra et al., 2023; Rathore et al., 2025). The observed PGEs with elevated condensation sinks (>0.1 s^{-1}) in Lucknow's highly polluted environment align with findings from Chinese megacities, where high CS values signify increased scavenging of gaseous precursors, such as sulfuric acid and organics, by preexisting aerosols, yet still permit growth dynamics (Du et al., 2022; Tuovinen et al., 2020).

BBOA-1 (fresh BB, high m/z 60) correlates strongly with nitrate (r=0.66) at Site 1 via regional stagnant chemistry, but weakly (r=0.26) at Site 2 due to local NOx overriding BB signals—directly tying secondary nitrate formation to apportioned BBOA transport.

O-BBOA (high f44, r=0.24 with m/z 60) at Site3 reflects processed BB organics growing via industrial vapors, explaining winter nighttime PGE maxima (5–15 nm/h) present at industrial Sites(Sarangi et al., 2018).

PMF source apportionment reveals distinct organic aerosol compositions across Lucknow Sites during the highly polluted post-monsoon period, directly linking to Site-specific dynamics observed in this study. At the Site1 (CSIR-CIMAP), SO_4-OA (28%), LV-OOA (24%), and BBOA-2 (13%) dominate, driven by regional nitrate-BBOA co-variation (r=0.66) that fosters secondary OA buildup under stagnant conditions. The Site 2 (BBAU) features LV-OOA (32%) and BBOA-1 (20%), with weak nitrate decoupling (r=0.26) from local NOx emissions overriding BB signals amid traffic's 50–60% contribution to ultrafine particle number concentration (PNC). At the Site 3 (Talkatora), O-BBOA (20%) and NO_3-OA (19%) prevail, enhanced by nocturnal particle growth events (5–15 nm/h) where stack vapors process BB organics (f60 r=0.24) under winter inversions. These hyperlocal patterns explain the dominance of organics (64–70% of NR-$PM_{2.5}$), underscoring the value of PMF for targeted controls on traffic PNC, regional precursors, and industrial emissions in the Indo-Gangetic Plain.

Traffic drives daytime particle number concentration via direct ultrafine emissions, but experience higher dispersion and scavenging at night, thereby suppressing PGEs during the post-monsoon period. Industrial Sites show less dilution and more persistent chemistry.
In the Indo-Gangetic Plain, during winters (e.g., Lucknow), nighttime PGEs are linked to industrial plumes under inversion layers, with growth rates enhanced by SO2/NOx emissions from stacks (Sarangi et al., 2018). These studies emphasize that polluted urban Sites with substantial aerosol loading exhibit enhanced vapor removal, which influences nucleation and growth processes, consistent with the current results.

https://doi.org/10.5194/egusphere-2026-595
Preprint. Discussion started: 13 March 2026

4. Conclusion

Overall, this study presents around 31 days of hyperlocal sampling across the CIGP city during the most polluted period (post-monsoon to winter) at three Sites representing distinct environmental conditions. For the first time in an Indian urban setting, a VSAAQMP platform was deployed to obtain high-resolution measurements of $PM_{2.5}$ composition and to perform source apportionment using a robust PMF approach coupled with the ME-2 engine, supported by collocated reference-grade instruments that strengthened the reliability of the observations. Using these near-source hyperlocal measurements collected in the post-monsoon to winter season of 2023 at multiple intra-city locations, the work investigates C-$PM_{2.5}$ levels in detail and yields the following key findings:

a)We found that during the highly polluted post-monsoon period, organics accounted for the largest contribution at all Sites, ranging from 64% to 70%. This was followed by nitrate (4–9%), sulfate (8–10%), ammonium (4–6%), and chloride (1–2%), while the refractory component, black carbon (BC), ranged from 4% to 17%. BC and sulfate (SO4) dominance at the clean/urban background site (Site 1) suggests regional/long-range transport and minimal local influence, whereas chloride (Chl), nitrate, and ammonia at the highly polluted Site 3 indicate intense local primary emissions and secondary aerosol formation under high-pollution conditions.

b)At Site 1, SO_4-OA (28.2 %) and LV-OOA (24.0 %) were the largest contributors, with additional contributions from BBOA-2 (12.9 %), SV-OOA (10.1 %), BBOA-1 (10.1 %), NO_3-OA (11.2 %), and a smaller share from HOA (3.5 %). At Site 2, LV-OOA (31.6 %) and SO_4-OA (20.7 %) again dominated, followed by BBOA-1 (20.3 %), NO_3-OA (14.1 %), BBOA-2 (7.7 %), and HOA (5.7 %). At Site 3, O-BBOA (20 %), SV-OOA (18.6 %), NO_3-OA (19 %), and LV-OOA (17.9 %) accounted for most of the organic mass, with additional contributions from solid fuel combustion (SFC) (10 %), SO_4-OA (7.6 %), and HOA (6.9 %).

c) The strong correlation observed between SO_4-OA and RH indicates that aqueous-phase processing significantly contributes to SO_4-OA formation during nighttime. This process was most pronounced at the highly polluted Site 3, followed by moderate activity at Site 2, and was least evident at the cleaner Site 1. Additionally, photochemical production was more prominent during the daytime at Site 3 than at Sites 1 and 2. In summary, at the highly polluted Site, diurnal variation in SO_4-OA indicates that photochemical processes dominate during the day, while aqueous-phase chemistry is more influential at night. In contrast, at less- and moderately polluted Sites, both mechanisms contribute to SO_4-OA formation throughout the day and night.

d)At Site 3, the CS varies from 0.1 to 0.7 s^{-1}, indicating a strong scavenging rate for gaseous precursors such as sulfuric acid and organic vapors—conditions typical of Lucknow's highly polluted urban environment. Hyperlocal PMF source apportionment across Lucknow's background (Site1), traffic (Site2), and industrial (Site3) Sites during the post-monsoon period elucidates organics' dominance (64–70% NR-PM_1) through distinct mechanisms: regional secondary buildup of SO_4-OA (28%) and LV-OOA (24%) via nitrate-BBOA co-variation (r=0.66) at Site 1; traffic-fueled nucleation into LV-OOA (32%) and BBOA-1 (20%) with NOx decoupling (r=0.26) at Site 2; and industrial vapor-driven nocturnal PGEs (5–15 nm/h) processing O-BBOA (20%, f60 r=0.24) at Site 3.

https://doi.org/10.5194/egusphere-2026-595
Preprint. Discussion started: 13 March 2026

e)Our analysis indicates that local and regional sources contributed 43.4% and 56.6%, respectively, across three measurement Sites, showing the strong background/transboundary influence.

f)The results indicate that particle growth events in the study domain are strongly controlled by pollution level and nocturnal secondary aerosol formation. A majority of PGEs occur at the most polluted Site, and about 53% take place at night, coinciding with high contributions from biomass-burning OA (BBOA), low-volatility oxygenated OA (LV-OOA), and nitrate-associated OA (NO_3-OA) at Sites 2 and 3. This implies that abundant organic precursors from combustion sources, together with nocturnal oxidants and shallow boundary layers(~250m-700m), efficiently drive nighttime SOA formation(as O: C ratio was high) and condensation-driven particle growth(as CS was higher), whereas the cleaner background Site, with weaker BBOA/LV-OOA influence, exhibits far fewer growth events. Thus, polluted C-IGP environments strongly enhance secondary aerosol formation and particle growth, whereas the cleaner background Site lacks sufficient precursors to sustain frequent growth events. These findings align with observations from the northern IGP studies.

These findings underscore the value of advanced PMF in resolving urban OA heterogeneity beyond bulk compositions, highlighting the need for traffic PNC controls, industrial vapor mitigation, and sustained high-resolution AMS/SMPS networks to address the impacts on air quality/climate in the Indo-Gangetic Plain. These regional influences in the background Site highlight the need for an integrated approach that combines regional airshed management with targeted hyperlocal interventions. Temporal analysis of $PM_{2.5}$ composition and sources, in conjunction with CWT analysis and meteorological conditions, suggests that transboundary emissions carried by prevailing winds from neighboring states significantly contribute to $PM_{2.5}$ in Lucknow. In contrast, hyperlocal monitoring at the most polluted Sites reveals substantial local contributions. Together, these findings demonstrate that effective air quality management must prioritize both coordinated regional controls and Site-specific, neighborhood-level measures, using hyperlocal data to design strategic, source-focused actions that protect human health and the environment. The novelty of the present work lies in its exploration of air quality at the hyperlocal level within the city scale. This type of hyperlocal measurement helps strategically target air pollution sources rather than implementing bulk measures. Additionally, more coordinated and systematic actions are essential to address air pollution in highly impacted areas.

Data availability

Data will be made available on request to the corresponding author.

Author contributions

DS designed the study, performed data analysis and conducted field investigations, developed methodology and software, conducted validation and formal analysis, and wrote the original draft with review and editing. AL performed data analysis and software, and conducted field investigations, with review and editing. AK, with review and editing,

https://doi.org/10.5194/egusphere-2026-595
Preprint. Discussion started: 13 March 2026

SC, HB, VJ, and SNT commented on and discussed the manuscript drafts. SNT provided supervision, resources, project administration, and funding acquisition. All authors reviewed and approved the final manuscript.

Competing interest

The contact author has declared that none of the authors has any competing interests.

Disclaimer

Copernicus Publications remains neutral with regard to jurisdictional claims made in the text, published maps, institutional affiliations, or any other geographical representation in this paper

Acknowledgements

We express our gratitude to CSIR-CIMAP, BBAU, and RK Residency Hotel, Talkatora, for their assistance in establishing the campaign Sites.

Financial Support

We also sincerely acknowledge the financial support provided by the Clean Air Fund (CAF: grant no. 001296) and Rail India Technical and Economic Service (RITES: approval no. RITES/UI/RCED/CoE/IITK). Additionally, S.N.T. gratefully recognizes the J.C. Bose Fellowship (JCB/2020/000044) awarded by the Science and Engineering Research Board, Department of Science and Technology, Government of India.

References

AethLabs: MicroAeth AE51 Operating Manual, 2016.

Aiken, A. C., DeCarlo, P. F., Kroll, J. H., Worsnop, D. R., Huffman, J. A., Docherty, K. S., Ulbrich, I. M., Mohr, C., Kimmel, J. R., Sueper, D., Sun, Y., Zhang, Q., Trimborn, A., Northway, M., Ziemann, P. J., Canagaratna, M. R., Onasch, T. B., Alfarra, M. R., Prevot, A. S. H., Dommen, J., Duplissy, J., Metzger, A., Baltensperger, U., and Jimenez, J. L.: O/C and OM/OC Ratios of Primary, Secondary, and Ambient Organic Aerosols with High-Resolution Time-of-Flight Aerosol Mass Spectrometry, Environmental Science & Technology, 42, 4478–4485, 2008.

Akanksha, Sethi, D., Kumar, A., Bhowmik, H. S., and Tripathi, S. N.: Comparative study of organic sources in Lucknow , India : industrial vs . background site from on- site mobile laboratory measurements, in: European Aerosol Conference (EAC) 2025, 2025.

Aktypis, A., Sippial, D. J., Vasilakopoulou, C. N., Matrali, A., Kaltsonoudis, C., Simonati, A., Paglione, M., Rinaldi, M., Decesari, S., and Pandis, S. N.: Formation and chemical evolution of SOA in two different environments: A dual chamber study, 1–33, 2024.

Alas, H. D. C., Weinhold, K., Costabile, F., Ianni, A. Di, Müller, T., Pfeifer, S., Liberto, L. Di, Turner, J. R., and Wiedensohler, A.: Methodology for high-quality mobile measurement with focus on black carbon and particle mass concentrations, Atmospheric Measurement Techniques, 12, 4697–4712, 2019.

Alas, H. D. C., Müller, T., Weinhold, K., Pfeifer, S., Glojek, K., Gregorič, A., Močnik, G., Drinovec, L., Costabile,

https://doi.org/10.5194/egusphere-2026-595
Preprint. Discussion started: 13 March 2026

F., Ristorini, M., and Wiedensohler, A.: Performance of microAethalometers : Real-world Field Intercomparisons from Multiple Mobile Measurement Campaigns in Different Atmospheric Environments, Aerosol and Air Quality Research, 20, 2640–2653, 2020.

Allan, J. D., Delia, A. E., Coe, H., Bower, K. N., Alfarra, M. R., Jimenez, J. L., Middlebrook, A. M., Drewnick, F., Onasch, T. B., Canagaratna, M. R., Jayne, J. T., and Worsnop, D. R.: A generalised method for the extraction of chemically resolved mass spectra from Aerodyne aerosol mass spectrometer data, Journal of Aerosol Science, 35, 909–922, https://doi.org/10.1016/j.jaerosci.2004.02.007, 2004.

Awasthi, A., Sinha, B., Hakkim, H., Mishra, S., Mummidivarapu, V., Singh, G., Ghude, S. D., Soni, V. K., Nigam, N., Sinha, V., and Rajeevan, M. N.: Biomass-burning sources control ambient particulate matter, but traffic and industrial sources control volatile organic compound (VOC) emissions and secondary-pollutant formation during extreme pollution events in Delhi, Atmospheric Chemistry and Physics, 24, 10279–10304, https://doi.org/10.5194/acp-24-10279-2024, 2024.

Barmpounakis, E., Geroliminis, N., Beojone, C., Stokking, P., Urbano Escobar, R., Ferro Santiago, E., Hacibekiroğlu, Y., and Akyol Ergüner, E.: Real-time pollution City mAp thRough cOLlaborative sensIng aNd Analysis: Collaborative and dynamic urban air pollution monitoring, Lausanne, 1–39 pp., 2020.

Bhandari, S., Gani, S., Patel, K., Wang, D. S., Soni, P., Arub, Z., Habib, G., Apte, J. S., and Hildebrandt Ruiz, L.: Sources and atmospheric dynamics of organic aerosol in New Delhi, India: Insights from receptor modeling, Atmospheric Chemistry and Physics, 20, 735–752, https://doi.org/10.5194/acp-20-735-2020, 2020.

Bhattu, D., Tripathi, S. N., Bhowmik, H. S., Moschos, V., Lee, C. P., Rauber, M., Salazar, G., Abbaszade, G., Cui, T., Slowik, J. G., Vats, P., Mishra, S., Lalchandani, V., Satish, R., Rai, P., Casotto, R., Tobler, A., Kumar, V., Hao, Y., Qi, L., Khare, P., Szidat, S., Chen, Y., Cao, J., Baltensperger, U., and Uzu, G.: Local incomplete combustion emissions define the PM 2 . 5 oxidative potential in Northern India, Nature Communications, 15, 1–13, https://doi.org/10.1038/s41467-024-47785-5, 2024.

Bhowmik, H. S., Tripathi, S. N., Sahu, R., Shukla, A. K., Lalchandani, V., Talukdar, S., Tripathi, N., and Sahu, L.: Insights into the Regional Transport and Local Formation of Secondary Organic Aerosol in Delhi, India, Aerosol and Air Quality Research, 22, 1–11, https://doi.org/10.4209/aaqr.220113, 2022.

Brown, S. G., Eberly, S., Paatero, P., and Norris, G. A.: Methods for estimating uncertainty in PMF solutions: Examples with ambient air and water quality data and guidance on reporting PMF results, Science of the Total Environment, 518–519, 626–635, https://doi.org/10.1016/j.scitotenv.2015.01.022, 2015.

Budisulistiorini, S. H., Baumann, K., Edgerton, E. S., Bairai, S. T., Mueller, S., Shaw, S. L., Knipping, E. M., Gold, A., and Surratt, J. D.: Seasonal characterization of submicron aerosol chemical composition and organic aerosol sources in the southeastern United States: Atlanta, Georgia,and Look Rock, Tennessee, Atmospheric Chemistry and Physics, 16, 5171–5189, https://doi.org/10.5194/acp-16-5171-2016, 2016.

Canonaco, F., Crippa, M., Slowik, J. G., Baltensperger, U., and Prévôt, A. S. H.: SoFi, an IGOR-based interface for the efficient use of the generalized multilinear engine (ME-2) for the source apportionment: ME-2 application to aerosol mass spectrometer data, Atmospheric Measurement Techniques, 6, 3649–3661, https://doi.org/10.5194/amt-6-3649-2013, 2013.

https://doi.org/10.5194/egusphere-2026-595
Preprint. Discussion started: 13 March 2026

Canonaco, F., Slowik, J. G., Baltensperger, U., and Prévôt, A. S. H.: Seasonal differences in oxygenated organic aerosol composition : implications for emissions sources and factor analysis, Atmos. Chem. Phys, 15, 6993–7002, https://doi.org/10.5194/acp-15-6993-2015, 2015.

Cash, J. M., Langford, B., Di Marco, C., Mullinger, N. J., Allan, J., Reyes-Villegas, E., Joshi, R., Heal, M. R., Acton, W. J. F., Hewitt, C. N., Misztal, P. K., Drysdale, W., Mandal, T. K., Shivani, Gadi, R., Gurjar, B. R., and Nemitz, E.: Seasonal analysis of submicron aerosol in Old Delhi using high-resolution aerosol mass spectrometry: Chemical characterisation, source apportionment and new marker identification, Atmospheric Chemistry and Physics, 21, 10133–10158, https://doi.org/10.5194/acp-21-10133-2021, 2021.

Cash, J. M., Di Marco, C., Langford, B., Heal, M. R., Mandal, T. K., Sharma, S. K., Gurjar, B. R., and Nemitz, E.: Response of organic aerosol to Delhi's pollution control measures over the period 2011–2018, Atmospheric Environment, 315, https://doi.org/10.1016/j.atmosenv.2023.120123, 2023.

Chakraborty, A., Ervens, B., Gupta, T., and Tripathi, S. N.: Characterization of organic residues of size-resolved fog droplets and their atmospheric implications, Journal of Geophysical Research : Atmospheres, 121, 2016.

Chang, W. L., Bhave, P. V., Brown, S. S., Riemer, N., Stutz, J., and Dabdub, D.: Heterogeneous atmospheric chemistry, ambient measurements, and model calculations of N2O5: A review, Aerosol Science and Technology, 45, 665–695, https://doi.org/10.1080/02786826.2010.551672, 2011.

Chang, Y., Du, T., Song, X., Wang, W., Tian, P., Guan, X., Zhang, N., Wang, M., Guo, Y., Shi, J., and Zhang, L.: Changes in physical and chemical properties of urban atmospheric aerosols and ozone during the COVID-19 lockdown in a semi-arid region, Atmospheric Environment, 287, https://doi.org/10.1016/j.atmosenv.2022.119270, 2022.

Chen, W., Ye, Y., Hu, W., Zhou, H., Pan, T., Wang, Y., Song, W., Song, Q., Ye, C., Wang, C., Wang, B., Huang, S., Yuan, B., Zhu, M., Lian, X., Zhang, G., Bi, X., Jiang, F., Liu, J., Canonaco, F., Prevot, A. S. H., Shao, M., and Wang, X.: Real-Time Characterization of Aerosol Compositions, Sources, and Aging Processes in Guangzhou During PRIDE-GBA 2018 Campaign, Journal of Geophysical Research: Atmospheres, 126, 1–27, https://doi.org/10.1029/2021JD035114, 2021.

Cheng, Y. and Lin, M.: Real-Time Performance of the microAeth ® AE51 and the Effects of Aerosol Loading on Its Measurement Results at a Traffic Site, Aerosol and Air Quality Research, 13, 1853–1863, https://doi.org/10.4209/aaqr.2012.12.0371, 2013.

Crippa, M., Canonaco, F., Lanz, V. A., Äijälä, M., Allan, J. D., Carbone, S., Capes, G., Ceburnis, D., Dall'Osto, M., Day, D. A., DeCarlo, P. F., Ehn, M., Eriksson, A., Freney, E., Ruiz, L. H., Hillamo, R., Jimenez, J. L., Junninen, H., Kiendler-Scharr, A., Kortelainen, A. M., Kulmala, M., Laaksonen, A., Mensah, A. A., Mohr, C., Nemitz, E., O'Dowd, C., Ovadnevaite, J., Pandis, S. N., Petäjä, T., Poulain, L., Saarikoski, S., Sellegri, K., Swietlicki, E., Tiitta, P., Worsnop, D. R., Baltensperger, U., and Prévôt, A. S. H.: Organic aerosol components derived from 25 AMS data sets across Europe using a consistent ME-2 based source apportionment approach, Atmospheric Chemistry and Physics, 14, 6159–6176, https://doi.org/10.5194/acp-14-6159-2014, 2014.

Daellenbach, K. R., Stefenelli, G., Bozzetti, C., Vlachou, A., Fermo, P., Gonzalez, R., Piazzalunga, A., Colombi, C., Canonaco, F., Hueglin, C., Kasper-Giebl, A., Jaffrezo, J. L., Bianchi, F., Slowik, J. G., Baltensperger, U., El-Haddad, I., and Prévôt, A. S. H.: Long-term chemical analysis and organic aerosol source apportionment at nine sites in central

https://doi.org/10.5194/egusphere-2026-595
Preprint. Discussion started: 13 March 2026

Europe: Source identification and uncertainty assessment, Atmospheric Chemistry and Physics, 17, 13265–13282, https://doi.org/10.5194/acp-17-13265-2017, 2017.

DeCarlo, P. F., Kimmel, J. R., Trimborn, A., Northway, M. J., Jayne, J. T., Aiken, A. C., Gonin, M., Fuhrer, K., Horvath, T., Docherty, K. S., Worsnop, D. R., and Jimenez, J. L.: Field-deployable, high-resolution, time-of-flight aerosol mass spectrometer, Analytical Chemistry, 78, 8281–8289, https://doi.org/10.1021/ac061249n, 2006.

DeWitt, H. L., Hellebust, S., Temime-Roussel, B., Ravier, S., Polo, L., Jacob, V., Buisson, C., Charron, A., André, M., Pasquier, A., Besombes, J. L., Jaffrezo, J. L., Wortham, H., and Marchand, N.: Near-highway aerosol and gas-phase measurements in a high-diesel environment, Atmospheric Chemistry and Physics, 15, 4373–4387, https://doi.org/10.5194/acp-15-4373-2015, 2015.

Dhandapani, S., Singh, P., Subbarao, S., and Jayachandran, K. S.: Catalysing Local Action for Clean Air A Guidebook to Map Hyperlocal Sources of Air Pollution, 2024.

Drosatou, A. D., Skyllakou, K., Theodoritsi, G. N., and Pandis, S. N.: Positive matrix factorization of organic aerosol : insights from a chemical transport model, Atmos. Chem. Phys, 19, 973–986, 2019.

Du, W., Cai, J., Zheng, F., Yan, C., Zhou, Y., Guo, Y., Chu, B., Yao, L., Heikkinen, L. M., Fan, X., Wang, Y., Cai, R., Hakala, S., Chan, T., Kontkanen, J., Tuovinen, S., Petäjä, T., Kangasluoma, J., Bianchi, F., Paasonen, P., Sun, Y., Kerminen, V. M., Liu, Y., Daellenbach, K. R., Dada, L., and Kulmala, M.: Influence of Aerosol Chemical Composition on Condensation Sink Efficiency and New Particle Formation in Beijing, Environmental Science and Technology Letters, 9, 375–382, https://doi.org/10.1021/acs.estlett.2c00159, 2022.

Du, Z., Hu, M., Peng, J., Zhang, W., Zheng, J., Gu, F., Qin, Y., Yang, Y., Li, M., Wu, Y., Shao, M., and Shuai, S.: Comparison of primary aerosol emission and secondary aerosol formation from gasoline direct injection and port fuel injection vehicles, Atmospheric Chemistry and Physics, 18, 9011–9023, https://doi.org/10.5194/acp-18-9011-2018, 2018.

Faisal, M., Hazarika, N., Ganguly, D., Kumar, M., and Singh, V.: PM2.5 bound species variation and source characterization in the post-lockdown period of the Covid-19 pandemic in Delhi, Urban Climate, 46, https://doi.org/10.1016/j.uclim.2022.101290, 2022.

Florou, K., Papanastasiou, D. K., Pikridas, M., Kaltsonoudis, C., Louvaris, E., Gkatzelis, G. I., Patoulias, D., Mihalopoulos, N., and Pandis, S. N.: The contribution of wood burning and other pollution sources to wintertime organic aerosol levels in two Greek cities, Atmospheric Chemistry and Physics, 17, 3145–3163, https://doi.org/10.5194/acp-17-3145-2017, 2017.

Frederickson, L. B., Russell, H. S., Fessa, D., Khan, J., Schmidt, J. A., Johnson, M. S., and Hertel, O.: Hyperlocal air pollution in an urban environment - measured with low-cost sensors, Urban Climate, 52, https://doi.org/10.1016/j.uclim.2023.101684, 2023.

Gelaro, R., McCarty, W., Suárez, M. J., Todling, R., Molod, A., Takacs, L., Randles, C. A., Darmenov, A., Bosilovich, M. G., Reichle, R., Wargan, K., Coy, L., Cullather, R., Draper, C., Akella, S., Buchard, V., Conaty, A., da Silva, A. M., Gu, W., Kim, G. K., Koster, R., Lucchesi, R., Merkova, D., Nielsen, J. E., Partyka, G., Pawson, S., Putman, W., Rienecker, M., Schubert, S. D., Sienkiewicz, M., and Zhao, B.: The modern-era retrospective analysis for research and applications, version 2 (MERRA-2), Journal of Climate, 30, 5419–5454, https://doi.org/10.1175/JCLI-D-16-

https://doi.org/10.5194/egusphere-2026-595
Preprint. Discussion started: 13 March 2026

0758.1, 2017.

Ghosh, S., Biswas, J., Guttikunda, S., Roychowdhury, S., and Nayak, M.: An investigation of potential regional and local source regions affecting fine particulate matter concentrations in Delhi, India, Journal of the Air and Waste Management Association, 65, 218–231, https://doi.org/10.1080/10962247.2014.982772, 2015.

Good, N., Peel, J. L., Volckens, J., Collins, F., and Sciences, R. H.: An accurate filter loading correction is essential for assessing personal exposure to black carbon using an Aethalometer Nicholas, J Expo Sci Environ Epidemiol., 27, 409–416, https://doi.org/10.1038/jes.2016.71.An, 2018.

Gu, Y., Huang, R., Duan, J., Xu, W., Lin, C., Zhong, H., Wang, Y., Ni, H., Liu, Q., Xu, R., Wang, L., and Li, Y. J.: Multiple pathways for the formation of secondary organic aerosol in the North China Plain in summer, Atmospheric Chemistry and Physics, 5419–5433, 2023.

Hao, L. Q., Kortelainen, A., Romakkaniemi, S., Portin, H., Jaatinen, A., Leskinen, A., Komppula, M., Miettinen, P., Sueper, D., Pajunoja, A., Smith, J. N., Lehtinen, K. E. J., Worsnop, D. R., Laaksonen, A., and Virtanen, A.: Atmospheric submicron aerosol composition and particulate organic nitrate formation in a boreal forestland-urban mixed region, Atmospheric Chemistry and Physics, 14, 13483–13495, https://doi.org/10.5194/acp-14-13483-2014, 2014.

Hao, Y., Strähl, J., Khare, P., Cui, T., Schneider-Beltran, K., Qi, L., Wang, D., Top, J., Surdu, M., Bhattu, D., Bhowmik, H. S., Vats, P., Rai, P., Kumar, V., Ganguly, D., Szidat, S., Uzu, G., Jaffrezo, J. L., Elazzouzi, R., Rastogi, N., Slowik, J., Haddad, I. E., Tripathi, S. N., Prévôt, A. S. H., and Daellenbach, K. R.: Transported smoke from crop residue burning as the major source of organic aerosol and health risks in northern Indian cities during post-monsoon, Environment International, 202, https://doi.org/10.1016/j.envint.2025.109583, 2025.

Hu, W., Campuzano-Jost, P., Day, D. A., Croteau, P., Canagaratna, M. R., Jayne, J. T., Worsnop, D. R., and Jimenez, J. L.: Evaluation of the new capture vaporizer for aerosol mass spectrometers (AMS) through field studies of inorganic species, Aerosol Science and Technology, 51, 735–754, https://doi.org/10.1080/02786826.2017.1296104, 2017.

IMD: Climatology of Lucknow, climate of Lucknow, 1–80 pp., 2012.

IQAir: World Air Quality Report 2023, IQAir, 1–45, 2023.

Jaganathan, S., Stafoggia, M., Rajiva, A., Mandal, S., Dixit, S., de Bont, J., Wellenius, G. A., Lane, K. J., Nori-Sarma, A., Kloog, I., Prabhakaran, D., Prabhakaran, P., Schwartz, J., and Ljungman, P.: Estimating the effect of annual PM2·5 exposure on mortality in India: a difference-in-differences approach, The Lancet Planetary Health, 8, e987–e996, https://doi.org/10.1016/S2542-5196(24)00248-1, 2024.

Jain, V., Tripathi, N., Tripathi, S. N., Gupta, M., Sahu, L. K., Murari, V., Gaddamidi, S., Shukla, A. K., and Prevot, A. S. H.: Real-time measurements of non-methane volatile organic compounds in the central Indo-Gangetic basin, Lucknow, India: source characterisation and their role in O3 and secondary organic aerosol formation, Atmospheric Chemistry and Physics, 23, 3383–3408, https://doi.org/10.5194/acp-23-3383-2023, 2023.

Jain, V., Mukherjee, A., Banerjee, S., Madhwal, S., Rai, P., and Nand, S.: A hybrid approach for integrating micro-satellite images and sensors network-based ground measurements using deep learning for high-resolution prediction of fine particulate matter (PM 2 . 5) over an indian city , lucknow, Atmosperic Environment, 338, 2024.

Jayne, J. T., Leard, D. C., Zhang, X., Davidovits, P., Smith, K. A., Kolb, C. E., and Worsnop, D. R.: Development of

https://doi.org/10.5194/egusphere-2026-595
Preprint. Discussion started: 13 March 2026

an aerosol mass spectrometer for size and composition analysis of submicron particles, Aerosol Science and Technology, 33, 49–70, https://doi.org/10.1080/027868200410840, 2000.

Jimenez, J. L., Canagaratna, M. R., Donahue, N. M., Prevot, A. S. H., Zhang, Q., Kroll, H., Decarlo, P. F., Allan, J. D., Coe, H., Ng, N. L., Aiken, A. C., Docherty, K. S., Grieshop, A. P., Robinson, A. L., Duplissy, J., Smith, J. D., Wilson, K. R., Lanz, V. A., Hueglin, C., Sun, Y. L., Tian, J., Laaksonen, A., Raatikainen, T., Rautiainen, J., Vaattovaara, P., Ehn, M., Kulmala, M., Tomlinson, J. M., Collins, D. R., Cubison, M. J., and Dunlea, E. J.: Evolution of Organic Aerosols in the Atmosphere All use subject to https://about.jstor.org/terms Evolution of Organic Aerosols in the Atmosphere, Science, 326, 1525–1529, 2009.

Kaltsonoudis, C., Florou, K., Kodros, J. K., Jorga, S. D., Vasilakopoulou, C. N., Baliaka, H. D., Matrali, A., Aktypis, A., Georgopoulou, M. P., Nenes, A., and Pandis, S. N.: Significant contributions of fresh and aged biomass burning organic aerosol from residential burning in a wintertime urban environment, Atmospheric Environment, 343, https://doi.org/10.1016/j.atmosenv.2024.121018, 2025.

Kerckhoffs, J., Hofman, J., Khan, J., Adams, M. D., Blanco, M. N., deSouza, P., Durant, J. L., Faridi, S., Fruin, S., Hankey, S., Hassanvand, M. S., Hatzopoulou, M., Hoek, G., de Hoogh, K., Hudda, N., Kushwaha, M., Marshall, J. D., Minet, L., Patton, A. P., Petäjä, T., Peters, J., Presto, A. A., Shairsingh, K., Sheppard, L., Simon, M. C., Vakacherla, S., Ryswyk, K. Van, Poppel, M. Van, Vermeulen, R. C. H., Wegener, R., Yuan, Z., and Amini, H.: Mobile monitoring of air pollution − a position paper on use cases, good practices, challenges, and opportunities, Environment International, 202, https://doi.org/10.1016/j.envint.2025.109582, 2025.

Kerminen, V. M., Chen, X., Vakkari, V., Petäjä, T., Kulmala, M., and Bianchi, F.: Atmospheric new particle formation and growth: Review of field observations, Environmental Research Letters, 13, https://doi.org/10.1088/1748-9326/aadf3c, 2018.

Khare, P., Kurdieh, A. A., Hao, Y., Manousakas, M., Dada, L., Tobler, A., Schneider-beltran, K., Diapouli, E., Skiba, A., Styszko, K., Slowik, J. G., Pr, S. H., and Daellenbach, K. R.: Organic Solvents-Based Offline Aerosol Mass Spectrometry (SOff- AMS) for Comprehensive Chemical Characterization of Ambient Organic Aerosol, https://doi.org/10.1021/acs.est.5c08949, 2025.

Kompalli, S. K., Nair, V. S., Jayachandran, V., Gogoi, M. M., and Babu, S. S.: Particle number size distributions and new particle formation events over the northern Indian Ocean during continental outflow, Atmospheric Environment, 238, https://doi.org/10.1016/j.atmosenv.2020.117719, 2020.

Kuang, Y., He, Y., Xu, W., Yuan, B., Zhang, G., Ma, Z., Wu, C., Wang, C., Wang, S., Zhang, S., Tao, J., Ma, N., Su, H., Cheng, Y., Shao, M., and Sun, Y.: Photochemical Aqueous-Phase Reactions Induce Rapid Daytime Formation of Oxygenated Organic Aerosol on the North China Plain, Environment Science and Technology, 3849–3860, https://doi.org/10.1021/acs.est.9b06836, 2020.

Kumar Kompalli, S., Suresh Babu, S., Krishna Moorthy, K., M Gogoi, M., S Nair, V., and Prakash Chaubey, J.: The formation and growth of ultrafine particles in two contrasting environments: A case study, Annales Geophysicae, 32, 817–830, https://doi.org/10.5194/angeo-32-817-2014, 2014.

Kumar, V., Giannoukos, S., Haslett, S. L., Tong, Y., Singh, A., Bertrand, A., Lee, C. P., Wang, D. S., Bhattu, D., Stefenelli, G., Dave, J. S., Puthussery, J. V, Qi, L., Vats, P., Rai, P., Casotto, R., Satish, R., Mishra, S., Pospisilova,

https://doi.org/10.5194/egusphere-2026-595
Preprint. Discussion started: 13 March 2026

V., Mohr, C., and Bell, D. M.: Highly time-resolved chemical speciation and source apportionment of organic aerosol components in Delhi , India , using extractive electrospray ionization mass spectrometry, Atmospheric Chemistry and Physics, 7739–7761, 2022.

Lakra, A., Shukla, A. K., Bhowmik, H. S., Yadav, A. K., Jain, V., Murari, V., Gaddamidi, S., Lalchandani, V., and Tripathi, S. N.: Comparative analysis of winter composite-PM2.5 in Central Indo Gangetic Plain cities: Combined organic and inorganic source apportionment and characterization, with a focus on the photochemical age effect on secondary organic aerosol formation, Atmospheric Environment, 338, 120827, https://doi.org/10.1016/j.atmosenv.2024.120827, 2024.

Lakra, A., Kumar, A., Sethi, D., Bhowmik, H. S., Jain, V., and Tripathi, S. N.: High-resolution source apportionment and health risks of PM2.5-bound trace elements across a major Indian city: Seasonal and diurnal insights from a multi-site campaign using a mobile laboratory platform., Atmosperic Environment, 102850, 2025.

Lalchandani, V., Kumar, V., Tobler, A., M. Thamban, N., Mishra, S., Slowik, J. G., Bhattu, D., Rai, P., Satish, R., Ganguly, D., Tiwari, S., Rastogi, N., Tiwari, S., Močnik, G., Prévôt, A. S. H., and Tripathi, S. N.: Real-time characterization and source apportionment of fine particulate matter in the Delhi megacity area during late winter, Science of the Total Environment, 770, https://doi.org/10.1016/j.scitotenv.2021.145324, 2021.

Lalchandani, V., Srivastava, D., Dave, J., Mishra, S., Tripathi, N., Shukla, A. K., Sahu, R., Thamban, N. M., Gaddamidi, S., Dixit, K., Ganguly, D., Tiwari, S., Srivastava, A. K., Sahu, L., Rastogi, N., Gargava, P., and Tripathi, S. N.: Effect of Biomass Burning on PM2.5 Composition and Secondary Aerosol Formation During Post-Monsoon and Winter Haze Episodes in Delhi, Journal of Geophysical Research: Atmospheres, 127, 1–21, https://doi.org/10.1029/2021JD035232, 2022.

Lhotka, R., Pokorná, P., Vodička, P., Zíková, N., Chen, G. I., Prévôt, A. S. H., Mbengue, S., Schwarz, J., and Ždímal, V.: Influence of meteorological conditions and seasonality on PM1 and organic aerosol sources at a rural background site, Atmospheric Environment, 344, https://doi.org/10.1016/j.atmosenv.2025.121028, 2025.

Liu, J., Christensen, J. H., Ye, Z., Dong, S., Geels, C., Brandt, J., Nenes, A., Yuan, Y., and Im, U.: Impact of meteorology and aerosol sources on PM2.5 and oxidative potential variability and levels in China, Atmospheric Chemistry and Physics, 24, 10849–10867, https://doi.org/10.5194/acp-24-10849-2024, 2024a.

Liu, L., Hohaus, T., Franke, P., Lange, A. C., Tillmann, R., Fuchs, H., Tan, Z., Rohrer, F., Karydis, V., He, Q., Vardhan, V., Andres, S., Bohn, B., Holland, F., Winter, B., Wedel, S., Novelli, A., Hofzumahaus, A., Wahner, A., and Kiendler-Scharr, A.: Observational evidence reveals the significance of nocturnal chemistry in seasonal secondary organic aerosol formation, npj Climate and Atmospheric Science, 7, 1–11, https://doi.org/10.1038/s41612-024-00747-6, 2024b.

Lucknow, India Metro Area Population 1950-2025: https://www.macrotrends.net/global-metrics/cities/21318/lucknow/population, last access: 2 June 2025.

Maslouski, M., Jarosz-Krzemińska, E., Jagoda, P., and Adamiec, E.: A mobile car monitoring system as a supplementary tool for air quality monitoring in urban and rural environments: the case study from Poland, Scientific Reports, 13, 1–10, https://doi.org/10.1038/s41598-023-43095-w, 2023.

Matsumoto, K. and Tanaka, H.: Formation and dissociation of atmospheric particulate nitrate and chloride: An

https://doi.org/10.5194/egusphere-2026-595
Preprint. Discussion started: 13 March 2026

approach based on phase equilibrium, Atmospheric Environment, 30, 639–648, https://doi.org/10.1016/1352-2310(95)00290-1, 1996.

Minguillón, M. C., Ripoll, A., Pérez, N., Prévôt, A. S. H., Canonaco, F., Querol, X., and Alastuey, A.: Chemical characterization of submicron regional background aerosols in the western Mediterranean using an Aerosol Chemical Speciation Monitor, Atmospheric Chemistry and Physics, 15, 6379–6391, https://doi.org/10.5194/acp-15-6379-2015, 2015.

Mishra, S., Tripathi, S. N., Kanawade, V. P., Haslett, S. L., Dada, L., Ciarelli, G., Kumar, V., Singh, A., Bhattu, D., Rastogi, N., Daellenbach, K. R., Ganguly, D., Gargava, P., Slowik, J. G., Kulmala, M., Mohr, C., El-Haddad, I., and Prevot, A. S. H.: Rapid night-time nanoparticle growth in Delhi driven by biomass-burning emissions, Nature Geoscience, 16, 224–230, https://doi.org/10.1038/s41561-023-01138-x, 2023.

Mohr, C., DeCarlo, P. F., Heringa, M. F., Chirico, R., Slowik, J. G., Richter, R., Reche, C., Alastuey, A., Querol, X., Seco, R., Peñuelas, J., Jiḿenez, J. L., Crippa, M., Zimmermann, R., Baltensperger, U., and Prévôt, A. S. H.: Identification and quantification of organic aerosol from cooking and other sources in Barcelona using aerosol mass spectrometer data, Atmospheric Chemistry and Physics, 12, 1649–1665, https://doi.org/10.5194/acp-12-1649-2012, 2012.

Mushasha, R., Paez Jimenez, A., Dolmazon, V., Baumann, J., Jansen, A., Storozhenko, O. N., and El-Bcheraoui, C.: Existing operational standards for field deployments of rapid response mobile laboratories: a scoping review, Frontiers in Public Health, 12, 1–15, https://doi.org/10.3389/fpubh.2024.1455738, 2024.

Nuaaman, I., Li, S., Hayden, K. L., Onasch, T. B., Massoli, P., and Sueper, D.: Separating refractory and non-refractory particulate chloride and estimating chloride depletion by aerosol mass spectrometry in a marine environment, 2085–2118, https://doi.org/10.5194/acpd-15-2085-2015, 2015.

Paatero, P.: The Multilinear Engine—A Table-Driven, Least Squares Program for Solving Multilinear Problems, Including the n-Way Parallel Factor Analysis Model, Journal of Computational and Graphical Statistics, 8, 854–888, https://doi.org/10.1080/10618600.1999.10474853, 1999.

Paatero, P., Eberly, S., Brown, S. G., and Norris, G. A.: Methods for estimating uncertainty in factor analytic solutions, Atmospheric Measurement Techniques, 7, 781–797, https://doi.org/10.5194/amt-7-781-2014, 2014.

Pal, I., Kumar, A., and Sir, S.: Research Paper on Air Pollution in Lucknow, 5, 884–888, https://doi.org/10.35629/5252-0504884888, 2023.

Petit, J. E., Favez, O., Albinet, A., and Canonaco, F.: A user-friendly tool for comprehensive evaluation of the geographical origins of atmospheric pollution: Wind and trajectory analyses, Environmental Modelling and Software, 88, 183–187, https://doi.org/10.1016/j.envsoft.2016.11.022, 2017.

Poulain, L., Spindler, G., Birmili, W., Plass-Dülmer, C., Wiedensohler, A., and Herrmann, H.: Seasonal and diurnal variations of particulate nitrate and organic matter at the IfT research station Melpitz, Atmospheric Chemistry and Physics, 11, 12579–12599, https://doi.org/10.5194/acp-11-12579-2011, 2011.

PRS Legislative Research: Uttar Pradesh Budget Analysis 2025-26, New Delhi, 2025.

Pushpawela, B., Jayaratne, R., and Morawska, L.: Differentiating between particle formation and growth events in an urban environment, Atmospheric Chemistry and Physics, 18, 11171–11183, https://doi.org/10.5194/acp-18-11171-

https://doi.org/10.5194/egusphere-2026-595
Preprint. Discussion started: 13 March 2026

2018, 2018.

Rai, P., Furger, M., El Haddad, I., Kumar, V., Wang, L., Singh, A., Dixit, K., Bhattu, D., Petit, J. E., Ganguly, D., Rastogi, N., Baltensperger, U., Tripathi, S. N., Slowik, J. G., and Prévôt, A. S. H.: Real-time measurement and source apportionment of elements in Delhi's atmosphere, Science of the Total Environment, 742, 1–16, https://doi.org/10.1016/j.scitotenv.2020.140332, 2020.

Rathore, J., Ganguly, D., Singh, V., Gupta, M., Vazhathara, V. J., Biswal, A., Kunchala, R. K., Patra, P. K., Sahu, L. K., Gani, S., and Dey, S.: Characteristics of Haze Pollution Events During Biomass Burning Period at an Upwind Site of Delhi, Journal of Geophysical Research: Atmospheres, 130, 1–26, https://doi.org/10.1029/2024JD042347, 2025.

Reyes-villegas, E., Green, D. C., Priestman, M., Canonaco, F., Coe, H., and Prévôt, A. S. H.: Organic aerosol source apportionment in London 2013 with ME-2 : exploring the solution space with annual and seasonal analysis, Atmos. Chem. Phys, 16, 15545–15559, https://doi.org/10.5194/acp-2016-465, 2016.

Ripoll, A., Minguillón, M. C., Pey, J., Jimenez, J. L., Day, D. A., Sosedova, Y., Canonaco, F., Prévôt, A. S. H., Querol, X., and Alastuey, A.: Long-term real-time chemical characterization of submicron aerosols at Montsec (southern Pyrenees, 1570 m a.s.l.), Atmospheric Chemistry and Physics, 15, 2935–2951, https://doi.org/10.5194/acp-15-2935-2015, 2015.

Roychowdhury, A., Somvanshi, A., and Kaur, S.: Urban Lab-Centre for Science and Environment Analysis Status of air quality monitoring in India: Spatial spread, population coverage and data completeness, New Delhi, India, 1–32 pp., 2023.

Saarikoski, S., Reyes, F., Vázquez, Y., Tagle, M., Timonen, H., Aurela, M., Carbone, S., Worsnop, D. R., Hillamo, R., and Oyola, P.: Characterization of submicron aerosol chemical composition and sources in the coastal area of Central Chile, Atmospheric Environment, 199, 391–401, https://doi.org/10.1016/j.atmosenv.2018.11.040, 2019.

Sarangi, B., Aggarwal, S. G., Kunwar, B., Kumar, S., Kaur, R., Sinha, D., Tiwari, S., and Kawamura, K.: Nighttime particle growth observed during spring in New Delhi: Evidences for the aqueous phase oxidation of SO2, Atmospheric Environment, 188, 82–96, https://doi.org/10.1016/j.atmosenv.2018.06.018, 2018.

Sathe, Y., Gupta, P., Bawase, M., Lamsal, L., and Patadia, F.: Since January 2020 Elsevier has created a COVID-19 resource centre with free information in English and Mandarin on the novel coronavirus COVID- 19 . The COVID-19 resource centre is hosted on Elsevier Connect , the company ' s public news and information, Sustainable Cities and Society, 66, 2020.

Schneider, I. L., Teixeira, E. C., Silva, L. F. O., and Wiegand, F.: Atmospheric particle number concentration and size distribution in a traffic–impacted area, Atmospheric Pollution Research, 6, 877–885, https://doi.org/10.5094/APR.2015.097, 2015.

Seinfeld, J. H. and S.Pandis: ATMOSPHERIC From Air Pollution to Climate Change SECOND EDITION, Second., JOHN WILEY & SONS, INC., 2006.

Shukla, A. K., Lalchandani, V., Bhattu, D., Dave, J. S., Rai, P., Thamban, N. M., Mishra, S., Gaddamidi, S., Tripathi, N., Vats, P., Rastogi, N., Sahu, L., Ganguly, D., Kumar, M., Singh, V., Gargava, P., and Tripathi, S. N.: Real-time quantification and source apportionment of fine particulate matter including organics and elements in Delhi during summertime, Atmospheric Environment, 261, 118598, https://doi.org/10.1016/j.atmosenv.2021.118598, 2021.

https://doi.org/10.5194/egusphere-2026-595
Preprint. Discussion started: 13 March 2026

Shukla, A. K., Tripathi, S. N., Talukdar, S., Murari, V., Gaddamidi, S., Manousakas, M.-I., Lalchandani, V., Dixit, K., Ruge, V. M., Khare, P., Kumar, M., Singh, V., Rastogi, N., Tiwari, S., Srivastava, A. K., Ganguly, D., Daellenbach, K. R., and Prévôt, A. S. H.: Measurement report: Sources and meteorology influencing highly time-resolved PM $_{2.5}$ trace elements at three urban sites in the extremely polluted Indo-Gangetic Plain in India, Atmospheric Chemistry and Physics, 25, 3765–3784, https://doi.org/10.5194/acp-25-3765-2025, 2025.

Squizzato, S., Masiol, M., Brunelli, A., Pistollato, S., Tarabotti, E., Rampazzo, G., and Pavoni, B.: Factors determining the formation of secondary inorganic aerosol: A case study in the Po Valley (Italy), Atmospheric Chemistry and Physics, 13, 1927–1939, https://doi.org/10.5194/acp-13-1927-2013, 2013.

Srivastava, D., Favez, O., Bonnaire, N., Lucarelli, F., Haeffelin, M., Perraudin, E., Gros, V., Villenave, E., and Albinet, A.: Speciation of organic fractions does matter for aerosol source apportionment. Part 2: Intensive short-term campaign in the Paris area (France), Science of the Total Environment, 634, 267–278, https://doi.org/10.1016/j.scitotenv.2018.03.296, 2018.

Sun, Y., Jiang, Q., Wang, Z., Fu, P., Li, J., Yang, T., and Yin, Y.: Journal of Geophysical Research : Atmospheres, Journal of Geophysical Research, 180–198, https://doi.org/10.1002/2013JD021040.Received, 2014.

Sun, Y. L., Zhang, Q., Schwab, J. J., Demerjian, K. L., Chen, W. N., Bae, M. S., Hung, H. M., Hogrefe, O., Frank, B., Rattigan, O. V., and Lin, Y. C.: Characterization of the sources and processes of organic and inorganic aerosols in New York city with a high-resolution time-of-flight aerosol mass apectrometer, Atmospheric Chemistry and Physics, 11, 1581–1602, https://doi.org/10.5194/acp-11-1581-2011, 2011.

Sun, Y. L., Zhang, Q., Schwab, J. J., Yang, T., Ng, N. L., and Demerjian, K. L.: Factor analysis of combined organic and inorganic aerosol mass spectra from high resolution aerosol mass spectrometer measurements, Atmospheric Chemistry and Physics, 12, 8537–8551, https://doi.org/10.5194/acp-12-8537-2012, 2012.

The Energy and Resources Institute: Estimation of Contribution of Sources to Ambient PM2.5 Concentration in Lucknow City, New Delhi, India, https://doi.org/10.56726/irjmets62296, 2022.

Tobler, A., Bhattu, D., Canonaco, F., Lalchandani, V., Shukla, A., Thamban, N. M., Mishra, S., Srivastava, A. K., Bisht, D. S., Tiwari, S., Singh, S., Močnik, G., Baltensperger, U., Tripathi, S. N., Slowik, J. G., and Prévôt, A. S. H.: Chemical characterization of PM2.5 and source apportionment of organic aerosol in New Delhi, India, Science of the Total Environment, 745, 1–12, https://doi.org/10.1016/j.scitotenv.2020.140924, 2020.

Tobler, A. K., Skiba, A., Canonaco, F., Močnik, G., Rai, P., Chen, G., Bartyzel, J., Zimnoch, M., Styszko, K., Nęcki, J., Furger, M., Rózański, K., Baltensperger, U., Slowik, J. G., and Prevot, A. S. H.: Characterization of non-refractory (NR) PM1and source apportionment of organic aerosol in Kraków, Poland, Atmospheric Chemistry and Physics, 21, 14893–14906, https://doi.org/10.5194/acp-21-14893-2021, 2021.

Tong, Y., Pospisilova, V., Qi, L., Duan, J., Gu, Y., Kumar, V., Rai, P., Stefenelli, G., Wang, L., Wang, Y., Zhong, H., Baltensperger, U., Cao, J., Huang, R. J., Prévôt, A. S. H., and Slowik, J. G.: Quantification of solid fuel combustion and aqueous chemistry contributions to secondary organic aerosol during wintertime haze events in Beijing, Atmospheric Chemistry and Physics, 21, 9859–9886, https://doi.org/10.5194/acp-21-9859-2021, 2021.

Tröstl, J., Chuang, W. K., Gordon, H., Heinritzi, M., Yan, C., Molteni, U., Ahlm, L., Frege, C., Bianchi, F., Wagner, R., Simon, M., Lehtipalo, K., Williamson, C., Craven, J. S., Duplissy, J., Adamov, A., Almeida, J., Bernhammer, A.

https://doi.org/10.5194/egusphere-2026-595
Preprint. Discussion started: 13 March 2026

K., Breitenlechner, M., Brilke, S., Dias, A., Ehrhart, S., Flagan, R. C., Franchin, A., Fuchs, C., Guida, R., Gysel, M., Hansel, A., Hoyle, C. R., Jokinen, T., Junninen, H., Kangasluoma, J., Keskinen, H., Kim, J., Krapf, M., Kürten, A., Laaksonen, A., Lawler, M., Leiminger, M., Mathot, S., Möhler, O., Nieminen, T., Onnela, A., Petäjä, T., Piel, F. M., Miettinen, P., Rissanen, M. P., Rondo, L., Sarnela, N., Schobesberger, S., Sengupta, K., Sipilä, M., Smith, J. N., Steiner, G., Tomè, A., Virtanen, A., Wagner, A. C., Weingartner, E., Wimmer, D., Winkler, P. M., Ye, P., Carslaw, K. S., Curtius, J., Dommen, J., Kirkby, J., Kulmala, M., Riipinen, I., Worsnop, D. R., Donahue, N. M., and Baltensperger, U.: The role of low-volatility organic compounds in initial particle growth in the atmosphere, Nature, 533, 527–531, https://doi.org/10.1038/nature18271, 2016.

TSI Incorporated: Electrostatic Classifier, Manual, B-2 to B-7 pp., 2006.

Tsimpidi, A. P., Scholz, S. M. C., Milousis, A., Mihalopoulos, N., and Karydis, V. A.: Aerosol Composition Trends during 2000-2020: In depth insights from model predictions and multiple worldwide observation datasets., Atmospheric Chemistry and Physics, 1–66, 2024.

Tuovinen, S., Kontkanen, J., Jiang, J., and Kulmala, M.: Investigating the effectiveness of condensation sink based on heterogeneous nucleation theory, Journal of Aerosol Science, 149, https://doi.org/10.1016/j.jaerosci.2020.105613, 2020.

Air Pollutant Receptor Modeling: https://www.epa.gov/scram/air-pollutant-receptor-modeling, last access: 4 March 2025.

U.S. Environmental Protection Agency: List of designated reference and equivalent methods, Research Triangle Park, NC, 2025.

Ulbrich, I. M., Canagaratna, M. R., Zhang, Q., Worsnop, D. R., and Jimenez, J. L.: Interpretation of organic components from Positive Matrix Factorization of aerosol mass spectrometric data, Atmospheric Chemistry and Physics, 9, 2891–2918, https://doi.org/10.5194/acp-9-2891-2009, 2009.

Vernooij, R., Winiger, P., Wooster, M., Strydom, T., Poulain, L., Dusek, U., Grosvenor, M., Roberts, G. J., Schutgens, N., and Werf, G. R. Van Der: A quadcopter unmanned aerial system (UAS) -based methodology for measuring biomass burning emission factors, Atmospheric Measurement Techniques, 15, 4271–4294, 2022.

Virkkula, A., Mäkelä, T., Hillamo, R., Yli-tuomi, T., Hirsikko, A., Hämeri, K., Koponen, I. K., Virkkula, A., and Ma, T.: A Simple Procedure for Correcting Loading Effects of Aethalometer Data A Simple Procedure for Correcting Loading Effects of Aethalometer Data, Journal of the Air & Waste Management Association, 57, 1214–1222, https://doi.org/10.3155/1047-3289.57.10.1214, 2012.

Vlachou, A., Daellenbach, K. R., Bozzetti, C., Chazeau, B., Salazar, G. A., Szidat, S., Jaffrezo, J. L., Hueglin, C., Baltensperger, U., El Haddad, I., and Prévôt, A. S. H.: Advanced source apportionment of carbonaceous aerosols by coupling offline AMS and radiocarbon size-segregated measurements over a nearly 2-year period, Atmospheric Chemistry and Physics, 18, 6187–6206, https://doi.org/10.5194/acp-18-6187-2018, 2018.

Wang, F., Zhang, X., Yue, X., Song, M., Zhang, G., and Ming, J.: Black carbon: The concentration and sources study at the Nam Co Lake, the Tibetan Plateau from 2015 to 2016, Atmosphere, 11, https://doi.org/10.3390/atmos11060624, 2020.

Wang, F., Zhang, C., Ge, Y., Zhang, Z., Shi, G., and Feng, Y.: Multi-scale analysis of the chemical and physical

https://doi.org/10.5194/egusphere-2026-595
Preprint. Discussion started: 13 March 2026

pollution evolution process from pre-co-pollution day to PM2.5 and O3 co-pollution day, Science of the Total Environment, 945, 1–10, https://doi.org/10.1016/j.scitotenv.2024.173729, 2024.

Wang, H., Lu, K., Chen, X., Zhu, Q., Wu, Z., Wu, Y., and Sun, K.: Fast particulate nitrate formation via N2O5 uptake aloft in winter in Beijing, Atmospheric Chemistry and Physics, 18, 10483–10495, https://doi.org/10.5194/acp-18-10483-2018, 2018.

Watson, J. G., Zhu, T., Chow, J. C., Engelbrecht, J., Fujita, E. M., and Wilson, W. E.: Receptor modeling application framework for particle source apportionment, Chemosphere, 49, 1093–1136, https://doi.org/10.1016/S0045-6535(02)00243-6, 2002.

Watson, T., Aiken, A., Zhang, Q., Croteau, P., Onasch, T., Williams, L., and Flynn, C.: Second ARM Aerosol Chemical Speciation Monitor Users ' Meeting Report, 2020.

Weingartner, E., Saathoff, H., Schnaiter, M., Streit, N., Bitnar, B., and Baltensperger, U.: Absorption of light by soot particles: Determination of the absorption coefficient by means of aethalometers, Journal of Aerosol Science, 34, 1445–1463, https://doi.org/10.1016/S0021-8502(03)00359-8, 2003.

Xu, L., Middlebrook, A. M., Liao, J., de Gouw, J. A., Guo, H., Weber, R. J., Nenes, A., Lopez-Hilfiker, F. D., Lee, B. H., Thornton, J. A., Brock, C. A., Neuman, J. A., Nowak, J. B., Pollack, I. B., Welti, A., Graus, M., Warneke, C., and Ng, N. L.: Enhanced formation of isoprene-derived organic aerosol in sulfur-rich power plant plumes during Southeast Nexus, Journal of Geophysical Research Atmospheres, 121, 9849–9861, https://doi.org/10.1002/2016JD025156.Received, 2016.

Xu, W., Xie, C., Karnezi, E., Zhang, Q., Wang, J., Pandis, S. N., Ge, X., Zhang, J., An, J., Wang, Q., Zhao, J., Du, W., Qiu, Y., Zhou, W., He, Y., Li, Y., Li, J., Fu, P., Wang, Z., Worsnop, D. R., and Sun, Y.: Summertime aerosol volatility measurements in Beijing, China, Atmospheric Chemistry and Physics, 19, 10205–10216, https://doi.org/10.5194/acp-19-10205-2019, 2019.

Yue, D., Hu, M., Wu, Z., Wang, Z., Guo, S., Wehner, B., Nowak, A., Achtert, P., Wiedensohler, A., Jung, J., Kim, Y. J., and Liu, S.: Characteristics of aerosol size distributions and new particle formation in the summer in Beijing, Journal of Geophysical Research Atmospheres, 114, 1–13, https://doi.org/10.1029/2008JD010894, 2009.

Yun, H., Wang, W., Wang, T., Xia, M., Yu, C., Wang, Z., C. N. Poon, S., Yue, D., and Zhou, Y.: Nitrate formation from heterogeneous uptake of dinitrogen pentoxide during a severe winter haze in southern China, Atmospheric Chemistry and Physics, 18, 17515–17527, https://doi.org/10.5194/acp-18-17515-2018, 2018.

Zhang, J. K., Sun, Y., Liu, Z. R., Ji, D. S., Hu, B., Liu, Q., and Wang, Y. S.: Characterization of submicron aerosols during a month of serious pollution in Beijing, 2013, Atmospheric Chemistry and Physics, 14, 2887–2903, https://doi.org/10.5194/acp-14-2887-2014, 2014.

Zhang, Q., Jimenez, J. L., Canagaratna, M. R., Allan, J. D., Coe, H., Ulbrich, I., Alfarra, M. R., Takami, A., Middlebrook, A. M., Sun, Y. L., Dzepina, K., Dunlea, E., Docherty, K., DeCarlo, P. F., Salcedo, D., Onasch, T., Jayne, J. T., Miyoshi, T., Shimono, A., Hatakeyama, S., Takegawa, N., Kondo, Y., Schneider, J., Drewnick, F., Borrmann, S., Weimer, S., Demerjian, K., Williams, P., Bower, K., Bahreini, R., Cottrell, L., Griffin, R. J., Rautiainen, J., Sun, J. Y., Zhang, Y. M., and Worsnop, D. R.: Ubiquity and dominance of oxygenated species in organic aerosols in anthropogenically-influenced Northern Hemisphere midlatitudes, Geophysical Research Letters, 34, 1–6,

https://doi.org/10.5194/egusphere-2026-595
Preprint. Discussion started: 13 March 2026

https://doi.org/10.1029/2007GL029979, 2007.

Zhang, X. and McMurry, P. H.: Evaporative losses of fine particulate nitrates during sampling, Atmospheric Environment Part A, General Topics, 26, 3305–3312, https://doi.org/10.1016/0960-1686(92)90347-N, 1992.

Zhang, Y. J., Tang, L. L., Wang, Z., Yu, H. X., Sun, Y. L., Liu, D., Qin, W., Canonaco, F., Prévôt, A. S. H., Zhang, H. L., and Zhou, H. C.: Insights into characteristics, sources, and evolution of submicron aerosols during harvest seasons in the Yangtze River delta region, China, Atmospheric Chemistry and Physics, 15, 1331–1349, https://doi.org/10.5194/acp-15-1331-2015, 2015.

Zhao, Z., Wang, Q., Li, L., Han, Y., Ye, Z., Pongpiachan, S., Zhang, Y., Liu, S., Tian, R., and Cao, J.: Characteristics of PM2.5 at a high-altitude remote site in the southeastern margin of the tibetan plateau in premonsoon season, Atmosphere, 10, https://doi.org/10.3390/atmos10110645, 2019.

Zheng, Y., Cheng, X., Liao, K., Li, Y., Li, Y. J., Huang, R.-J., Hu, W., Liu, Y., Zhu, T., Chen, S., Zeng, L., Worsnop, D. R., and Chen, Q.: Characterization of anthropogenic organic aerosols by TOF-ACSM with the new capture vaporizer, Atmospheric Measurement Techniques, 13, 2457–2472, 2020.

Zimmerman, A., Petters, M. D., and Meskhidze, N.: Observations of new particle formation, modal growth rates, and direct emissions of sub-10 nm particles in an urban environment, Atmospheric Environment, 242, 2020.